nature communications

Article

https://doi.org/10.1038/s41467-024-55005-3

ATAD5-BAZ1B interaction modulates PCNA ubiquitination during DNA repair

Received: 29 January 2024

Accepted: 25 November 2024

Published online: 03 December 2024

Check for updates

Yeongjae Kim[1,2], Na Young Ha[1], Mi-Sun Kang[1], Eunjin Ryu[1,3], Geunil Yi[1,2], Juyeong Yoo[1,2], Nalae Kang[1], Byung-Gyu Kim[1], Kyungjae Myung[1,2] & Sukhyun Kang[1]

Mono-ubiquitinated PCNA (mono-Ub-PCNA) is generated when replication forks encounter obstacles, enabling the bypass of DNA lesions. After resolving stalled forks, Ub-PCNA must be de-ubiquitinated to resume high-fidelity DNA synthesis. ATAD5, in cooperation with the UAF1-USP1 complex, is responsible for this de-ubiquitination. However, the precise regulation of timely Ub-PCNA de-ubiquitination remains unclear. Our research reveals that BAZ1B, a regulatory subunit of the BAZ1B-SMARCA5 chromatin-remodeling complex (also known as the WICH complex), plays a crucial role in fine-tuning the de-ubiquitination process of Ub-PCNA. The BAZ1B binding region of ATAD5 encompasses the UAF1-binding domain of ATAD5. Disruption of the ATAD5-BAZ1B interaction results in premature de-ubiquitination of Ub-PCNA following treatment with hydrogen peroxide. Cells with impaired BAZ1B binding to ATAD5 display increased sensitivity to oxidative stress compared to wild-type cells. These findings suggest that BAZ1B prevents premature Ub-PCNA de-ubiquitination, thereby safeguarding genome integrity.

During DNA synthesis, replication machinery often encounters obstacles that stall replication forks. Various factors are then recruited to remove these obstacles or bypass DNA lesions[1–5]. Once the stalled forks are resolved, DNA repair and lesion bypass factors are released, allowing high-fidelity DNA replication to resume[6]. This dynamic process is essential for genome duplication but is not yet fully understood.

To circumvent DNA lesions, eukaryotic cells use proliferating cell nuclear antigen (PCNA)-mediated lesion bypass mechanisms[7–9]. PCNA forms a homo-trimeric ring that encircles DNA[10] and is loaded onto the primer-template junction by the Replication Factor-C complex (RFC) and the CTF18-containing RFC-like Complex (CTF18-RLC)[11–14]. During unchallenged DNA synthesis, PCNA tethers replicative DNA polymerases, enhancing their processivity[15,16]. When replicative polymerases are stalled by DNA lesions, PCNA is mono-ubiquitinated at residue K164 by RAD6-RAD18.

The ubiquitination of PCNA (Ub-PCNA) is key to lesion bypass, recruiting translesion synthesis (TLS) DNA polymerases[17–19]. These polymerases can traverse DNA lesions but are characterized by low processivity and error-proneness. This mechanism allows the completion of DNA replication without leaving unreplicated gaps[20–22]. Following lesion bypass, Ub-PCNA is de-ubiquitinated and unloaded, terminating the bypass signal[23–25]. This step is controlled by the ATAD5-RLC, which, unlike the canonical RFC, unloads PCNA from DNA[26–28]. Both ATAD5-RLC and RFC are pentameric complexes sharing four small subunits (RFC2–5), with RFC1 and ATAD5 conferring the PCNA-loading and unloading activities, respectively[12,29–31].

ATAD5 can be divided into two functional domains (Supplementary Fig. 1a): the N-terminal one-third (ATAD5-N) and the remaining C-terminal two-thirds (ATAD5-C)[28]. ATAD5-C contains an AAA+ ATPase domain and forms the PCNA-unloading complex with RFC2–5[27,28]. ATAD5-N facilitates the de-ubiquitination of Ub-PCNA through interaction with the de-ubiquitinase UAF1-USP1[32].

ATAD5-RLC is crucial for efficient PCNA recycling for subsequent rounds of DNA synthesis. Because of PCNA's critical roles in DNA

[1]Center for Genomic Integrity, Institute for Basic Science, Ulsan 44919, Republic of Korea. [2]Department of Biological Sciences, Ulsan National Institute of Science and Technology, Ulsan 44919, Republic of Korea. [3]Present address: Department of Biological Chemistry and Molecular Pharmacology, Blavatnik Institute, Harvard Medical School, 240 Longwood Avenue, Boston, MA 02115, USA. e-mail: kangsh@ibs.re.kr

synthesis, its unloading and de-ubiquitination must be tightly regulated to prevent premature removal from DNA. We previously demonstrated that PCNA-interacting replication proteins inhibit PCNA unloading during DNA synthesis[28,33]. We also showed that the chromatin reader BRD4 negatively regulates the PCNA-unloading activity of ATAD5-RLC[33]. However, how ATAD5 modulates Ub-PCNA de-ubiquitination to timely terminate DNA lesion bypass synthesis remains unclear.

Chromatin-remodeling complexes are essential for DNA replication and repair. They facilitate nucleosome redistribution, allowing access to DNA during replication and repair[34–40]. Among these remodelers, BAZ1B-SMARCA5 interacts with PCNA and remodels nascent chromatin during DNA replication. It belongs to the ISWI family of chromatin remodelers[41,42], where BAZ1B acts as the regulatory subunit and SMARCA5 as the catalytic subunit with nucleosome-remodeling activity[43]. BAZ1B localizes to replication foci in the S phase through interaction with PCNA. BAZ1B depletion results in compacted nascent chromatin and increased heterochromatin markers[41]. Additionally, BAZ1B associates with pericentric heterochromatin, indicating a role in heterochromatin replication[42]. As a component of the transcription-regulating complex B-WICH, BAZ1B-SMARCA5 influences transcription by altering chromatin structure around ribosomal DNA and modulating acetyl-histone marks[44–48]. Furthermore, BAZ1B is involved in DNA repair. BAZ1B-SMARCA5 is recruited to UV-C-induced DNA damage sites, and its loss impairs recovery from DNA damage[49]. The BAZ1B N-terminal domain has atypical tyrosine kinase activity, phosphorylating Y142 of H2AX, maintaining S139 phosphorylation of H2AX during DNA damage[50].

In this study, we discovered an unexpected function of BAZ1B in DNA lesion bypass regulation. BAZ1B interacts with the de-ubiquitination domain of ATAD5, negatively regulating Ub-PCNA de-ubiquitination. Disruption of the ATAD5-BAZ1B interaction leads to premature Ub-PCNA de-ubiquitination and increased DNA damage under oxidative stress. Our findings suggest that BAZ1B fine-tunes the ubiquitination status of PCNA, ensuring the appropriate resolution of DNA lesions.

Results

BAZ1B-SMARCA5 interacts with ATAD5

It is well established that ATAD5-RLC is responsible for unloading PCNA and that ATAD5 interacts with the UAF1-USP1 complex to facilitate the de-ubiquitination of Ub-PCNA. However, the precise mechanisms by which ATAD5 regulates PCNA cycling are not fully elucidated. We hypothesized that proteins binding to ATAD5 may regulate its activity. To evaluate this hypothesis, we isolated proteins that interact with ATAD5 (Fig. 1a). To enrich the ATAD5 interactome, we integrated a lentiviral expression cassette encoding CLIP-ATAD5-StrepII-FLAG into an ATAD5 knock-out 293 T cell line. ATAD5 was isolated using Strep-Tactin beads, and co-isolated proteins were analyzed through mass spectrometry. As anticipated, the small RFC subunits, RFC2–5, were enriched with ATAD5. Additionally, BET proteins, known to regulate the PCNA-unloading activity of ATAD5-RLC, were identified in the ATAD5 interactome[5,33]. Consistent with prior studies, UAF1-USP1 co-purified with ATAD5, reinforcing the role of ATAD5 in Ub-PCNA de-ubiquitination[32]. Notably, the ISWI chromatin remodeler complex BAZ1B-SMARCA5 was also enriched with ATAD5. The interaction between ATAD5 and BAZ1B was confirmed via co-immunoprecipitation of BAZ1B with ATAD5 (Fig. 1b). To corroborate this interaction further, we transiently expressed BAZ1B-FLAG and isolated BAZ1B-interacting proteins using anti-FLAG beads (Fig. 1c). ATAD5 was identified in the BAZ1B interactome along with SMARCA5, PCNA, and SIRT1[41–43,51]. Immunoprecipitation assays revealed that ATAD5 co-immunoprecipitated with both exogenously expressed and endogenous BAZ1B (Fig. 1d, e), indicating a physiological interaction.

Next, we explored which component of the BAZ1B-SMARCA5 complex interacts with ATAD5. Depletion of BAZ1B significantly reduced ATAD5 co-precipitation in the SMARCA5 pull-down assay (Fig. 1f). Furthermore, the BAZ1B-binding defective SMARCA5 mutant (ΔSLIDE)[49] did not interact with ATAD5 (Supplementary Fig. 1b), indicating that the interaction occurs through BAZ1B.

Finally, we assessed whether DNA-damaging agents influence the ATAD5-BAZ1B interaction. Treatment with hydrogen peroxide, UV, hydroxyurea (HU), and camptothecin (CPT) did not disrupt the interaction (Fig. 1g, Supplementary Fig. 1c, d).

The ATAD5 de-ubiquitination domain interacts with BAZ1B-SMARCA5

ATAD5 exhibits two key biochemical functions: unloading PCNA and facilitating the de-ubiquitination of Ub-PCNA, which are mediated by its C-terminal and N-terminal domains, respectively[28,32]. To explore whether the functions of ATAD5 are regulated by the BAZ1B-SMARCA5 complex, we examined the BAZ1B-binding region of ATAD5 (Fig. 2, Supplementary Fig. 2). We found that the N-terminal domain of ATAD5, specifically residues 1–692, interacted with BAZ1B (Fig. 2a). This domain interacts with various proteins, including UAF1 and BRD4, through distinct motifs. By analyzing deletion variants of ATAD5 (1–692), we were able to define the BAZ1B-binding region more precisely (Fig. 2b). Deletion of residues 240–320 completely abolished the BAZ1B interaction without affecting the binding of UAF1 or BRD4. Removing residues 400–693 resulted in partial reduction in BAZ1B binding. Although ATAD5 (400–693) contains a motif for BET protein binding[33], a BET-binding defective mutation did not impair BAZ1B binding (Supplementary Fig. 2a), suggesting that this region enhances BAZ1B binding independently of BET proteins. Therefore, the BAZ1B binding region overlaps with the UAF1-binding domain of ATAD5.

To further comprehend the ATAD5-BAZ1B interaction, we identified specific mutations in ATAD5 that disrupt BAZ1B binding. Mutating the conserved residues ^{264}TVSYEEF^{270} to AVAYAA (referred to as ATAD5 B1m) completely abolished BAZ1B binding (Fig. 2c, Supplementary Fig. 2b). The K272A mutation also weakened this interaction, whereas the S261A mutation did not. The BAZ1B-binding motif of ATAD5 contains a conserved serine at position 266 (S266). Notably, the S266A mutation increased the mobility of ATAD5 (1–500) in SDS-PAGE and reduced BAZ1B binding, whereas the S266D mutation behaved similarly to the wild-type both in mobility and binding (Supplementary Fig. 2c). Despite the sequence ^{264}SYEE^{267} resembling a CKII consensus site (S-x-x-E), CKII depletion did not affect the interaction between BAZ1B and ATAD5 (Supplementary Fig. 2d). These findings suggest that S266 might be phosphorylated by a kinase other than CKII, enhancing BAZ1B binding. Furthermore, the B1m mutation in full-length ATAD5 specifically abrogated the binding of the BAZ1B-SMARCA5 complex without affecting UAF1 or BRD4 binding (Fig. 2d), identifying the ATAD5 B1 motif as the primary BAZ1B binding interface (Supplementary Fig. 2e).

The BAZ1B N-terminal domain interacts with ATAD5

We explored which region of BAZ1B interacts with ATAD5 (Fig. 3a). BAZ1B contains an N-terminal WSTF/Acf1/cbp146 (WAC) domain, a middle DNA-binding homeobox-containing proteins and different transcription and chromatin remodeling factors (DDT) domain, and a C-terminal bromodomain. To determine the ATAD5-binding domain, we expressed various BAZ1B deletion variants and performed immunoprecipitation (Fig. 3a). Deletion of residues 1–500 in BAZ1B abolished its interaction with ATAD5, indicating that ATAD5 binds to the N-terminal region of BAZ1B. While prior research has shown that the N-terminal domain of BAZ1B exhibits tyrosine kinase activity for H2AX Y142[50], other binding partners for this domain have not been reported. Our detailed examination of the N-terminal region identified residues 42–365 of BAZ1B as crucial for binding to ATAD5 (Supplementary Fig. 3a). This

a

CLIP-ATAD5-FLAG-StrepII

↓

StrepII IP & Mass Spec.

	Peptide numbers	
	Mock	ATAD5
ATAD5	0	62
RFC5	0	21
RFC3	0	18
RFC2	0	18
RFC4	0	16
UAF1	0	15
USP1	0	2
USP7	0	1
BAZ1B	0	6
SMARCA5	0	5
BRD4	0	9
BRD2	0	4
BRD3	0	2

Peptides co-isolated with ATAD5-StrepII

c

BAZ1B-FLAG

↓

FLAG IP & Mass Spec.

	Peptide numbers	
	Mock	BAZ1B
BAZ1B	6	360
SMARCA5	4	63
SMARCA1	0	18
SIRT1	0	17
PCNA	0	6
ATAD5	0	2

Peptides co-isolated with BAZ1B-FLAG

b

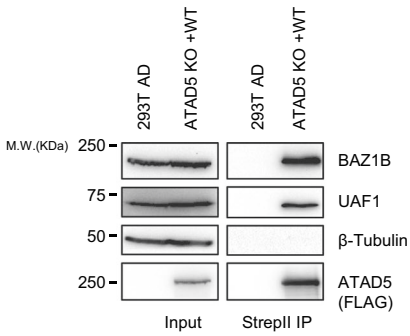

d

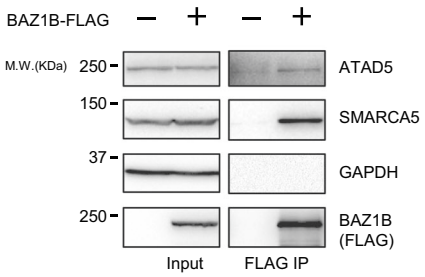

e

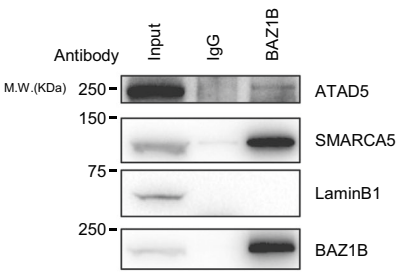

f

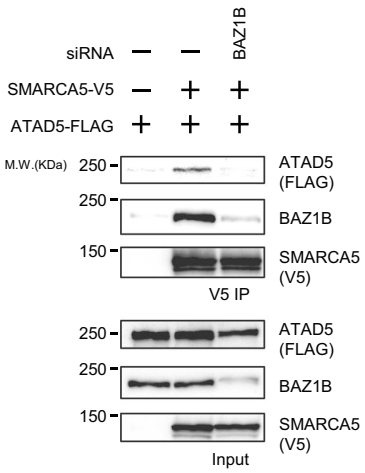

g

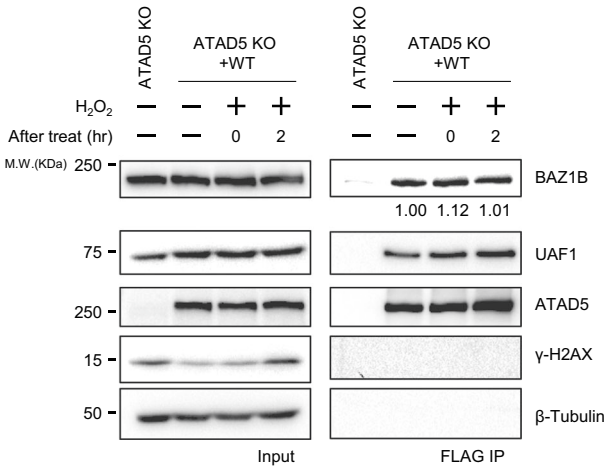

region is highly conserved across species, and deletions within this domain decreased the stability of transiently expressed BAZ1B in cells. Through alanine scanning of the N-terminal region, we identified two motifs, ^{118}EECDF^{122} (A5BM1) and ^{221}KYDVK^{225} (A5BM2), as important for interaction with ATAD5 (Fig. 3b, Supplementary Fig. 3b–f).

To further investigate the ATAD5-BAZ1B interaction, we conducted structural prediction analysis using AlphaFold2 (Supplementary Fig. 3g). The predictions suggest that the ATAD5 region encompassing residues 260–270 is critical for binding to BAZ1B. The BAZ1B binding region and the ATAD5 binding domain form a 4-stranded antiparallel structure. Notably, residues Y267 and F270 in the ATAD5 B1 motif engage in aromatic π-π interactions with the BAZ1B F122 residue (Supplementary Fig. 3h). These π-π stacking interactions are crucial for protein-protein interaction[52]. The ATAD5

Fig. 1 | BAZ1B interacts with ATAD5. a BAZ1B-SMARCA5 binds to ATAD5. ATAD5 was affinity-purified using Strep-Tactin beads from ATAD5 knock-out cells that re-express CLIP-ATAD5-FLAG-StrepII. The co-isolated proteins were identified through Mass Spectrometry. **b** BAZ1B is co-precipitated with ATAD5. ATAD5 was affinity purified from the indicated cells, and co-purified proteins were analyzed using immunoblotting. **c** ATAD5 binds to BAZ1B-SMARCA5. Transiently expressed BAZ1B-FLAG was immunoprecipitated using anti-FLAG beads and the co-isolated proteins were identified by Mass Spectrometry. BAZ1B binds to ATAD5. Transiently expressed BAZ1B-FLAG, (**d**), or endogenous BAZ1B, (**e**), was immunoprecipitated using anti-FLAG beads or anti-BAZ1B antibody, respectively. The isolated proteins were examined by immunoblotting. **f** BAZ1B depletion abolished the interaction between SMARCA5 and ATAD5. FLAG-ATAD5 and SMARCA5-V5 were transiently expressed, with or without BAZ1B depletion as indicated, to assess interactions. **g** Oxidative stress does not affect ATAD5-BAZ1B interaction. Wild-type ATAD5 cells were treated with 1 mM hydrogen peroxide for 20 min, followed by incubation in fresh media for the indicated time period. ATAD5 was immunoprecipitated using anti-FLAG beads. The numbers below the BAZ1B blot indicate the relative amount of BAZ1B co-precipitating. Source data are provided as a Source Data file.

(Y267A, F270A) mutation disrupted its interaction with BAZ1B, similar to the B1m mutant (Supplementary Fig. 3i, j). Furthermore, the F122A mutation in BAZ1B A5BM1 abolished the interaction with ATAD5, validating our predictions (Fig. 3c).

In AlphaFold2 prediction, A5BM1 and A5BM2 of BAZ1B are predicted to form β strands that constitute the ATAD5-binding domain. Another β strand, consisting of BAZ1B residues ^{231}KIIS^{234} and referred to as A5BM3, was found to align next to ATAD5 B1, forming parallel interactions (Supplementary Fig. 3k). Additionally, E118 in the BAZ1B A5BM1 motif stabilizes the orientation of the β-sheet-based motif towards ATAD5, strengthening the ATAD5-BAZ1B interaction. Y222 in the BAZ1B A5BM2 motif forms a T-shaped π-π stacking interaction with BAZ1B Y114, which stabilizes the positioning of A5BM1 to support the ATAD5-BAZ1B interaction (Supplementary Fig. 3k). Consistent with our predictions, the E118A, Y222A, and A5BM3 AAAA mutants showed significant defects in ATAD5 interaction (Fig. 3c, Supplementary Fig. 3b, l, m).

Consistent with previous reports, PCNA co-immunoprecipitated with BAZ1B (Fig. 3b, c). The ATAD5-binding defective BAZ1B mutation did not affect PCNA binding, suggesting that the PCNA-BAZ1B interaction occurs independently of ATAD5 (Fig. 3b). To explore whether PCNA influences the ATAD5-BAZ1B interaction, we searched for a PCNA-binding motif in BAZ1B. We identified that PCNA binds to BAZ1B (1–500), but not to BAZ1B (501–1000) or BAZ1B (1001–1483) (Supplementary Fig. 4a). Further analysis revealed that BAZ1B residues 323–466 are essential for PCNA binding (Fig. 3d). We tested several mutations within BAZ1B (323–466) and found that the mutation of ^{436}KQMTL^{440} to AAGAG (PIPm) eliminated the BAZ1B-PCNA interaction (Fig. 3e, Supplementary Fig. 4b, c). This PCNA-interacting motif (BAZ1B PIP) features a distinct peptide sequence compared to the canonical PIP box (Q-x-x-ψ-x-x-θ-θ). Notably, the PCNA-interaction mutant did not affect ATAD5 binding, indicating that ATAD5 binds to BAZ1B independently of PCNA.

Next, we prepared ubiquitin- and SUMO-fused PCNA to assess whether these modifications affect the BAZ1B-PCNA interaction. BAZ1B bound to ubiquitin-, SUMO1-, and SUMO2-fused PCNA with a similar affinity to unmodified PCNA, indicating that these modifications do not influence the BAZ1B-PCNA interaction (Supplementary Fig. 4d).

Regarding the SMARCA5 interaction, both the middle region of BAZ1B (residues 539–592, Supplementary Fig. 4e) and the C-terminal region (residues 1001–1483, Fig. 3a) were necessary. To further explore this interaction, we tested several mutations in the middle region of BAZ1B. We found that mutating residues ^{590}LPAF^{593} (referred to as S5BM1) to AAAA abolished SMARCA5 binding (Supplementary Fig. 4f–i). Mutations in the DDT or WHIM1-2 domains did not affect SMARCA5 binding, although a previous report suggested that the WHIM domains might be involved in SMARCA5 interaction[53]. For the C-terminal region, deleting the bromodomain did not impede its interaction with SMARCA5 (Supplementary Fig. 4j). Additional deletion mutants revealed that residues 1027–1214 contain the SMARCA5-binding motif (Supplementary Fig. 4k). Further mutational analysis of conserved patches within this region was conducted through immunoprecipitation (Supplementary Fig. 4l, m). This analysis indicated that mutating residues ^{1158}EAQTFSR^{1164} (referred to as S5BM2) to AAAAAAA eliminated the SMARCA5 interaction. Importantly, mutations in both S5BM1 and S5BM2 did not affect ATAD5 binding.

Overall, BAZ1B interacts with ATAD5 and PCNA through its N-terminal domain and with SMARCA5 through its middle and C-terminal domains. Notably, each protein interacts with BAZ1B independently (Supplementary Fig. 4n).

ATAD5 and BAZ1B are recruited to DNA synthesis sites by PCNA independently

Induction of DNA damage by micro-irradiation leads to the accumulation of replication and repair factors[54–56], including BAZ1B, ATAD5, and PCNA, at sites of damage (Fig. 4a, b, Supplementary Fig. 5a). Given that these proteins interact with each other, we investigated their recruitment to the micro-irradiated sites to understand their interplay. We observed that a PCNA-binding defective mutant of BAZ1B (BAZ1B PIPm) failed to localize to the sites of micro-irradiation (Fig. 4a). In contrast, mutations that disrupt ATAD5 interaction (BAZ1B F122A) or deletion of the bromodomain (BAZ1B ΔBromo) did not affect BAZ1B localization to DNA damage sites. This aligns with previous findings that a PCNA-interacting peptide interferes with BAZ1B localization to replication foci, suggesting that BAZ1B is recruited to replication forks by PCNA[41]. Our results confirm that direct interaction with PCNA is crucial for BAZ1B recruitment after DNA damage.

Similarly, ATAD5 rapidly localized DNA damage sites (Fig. 4b). The specific motif on ATAD5 responsible for this localization remains unidentified. We found that ATAD5 (1–692) localized to damage sites, whereas ATAD5 (693–1844), which includes the PCNA-unloading domain, did not. Further analysis showed that ATAD5 (1–400) targets DNA damage sites (Supplementary Fig. 5b). This region includes the BAZ1B binding motif, but the ATAD5 B1m mutation did not affect localization (Fig. 4c). Additionally, the UAF1 binding-defective ATAD5 (1–692) also localized to the damaged site (Supplementary Fig. 5c). The far N-terminus of ATAD5 contains conserved amino acids, and mutations in these residues (referred to as far N-terminal mutations, NTM) significantly reduced localization to damage sites (Fig. 4d, Supplementary Fig. 5d). Notably, the residues ^{61}NILDYF^{66} in the ATAD5 N-terminus resemble a predicted PCNA-interacting motif. Using AlphaFold2, we predicted the structure of the ATAD5 (1–603) bound to PCNA, revealing that ATAD5 residues ^{62}ILDYF^{66} were positioned in the binding pocket of IDCL of PCNA (Supplementary Fig. 5e). Based on this prediction, we generated an N-PIP mutant by substituting ^{62}ILDYF^{66} with ALDAA, finding that both the NTM and N-PIP mutant significantly reduced PCNA binding (Supplementary Fig. 5d, f). Interestingly, the localization to damage sites was also significantly impaired by the N-PIP mutation (Supplementary Fig. 5g). RFC1 depletion prevents the loading of PCNA onto DNA and reduces the PCNA accumulation at micro-irradiation sites[57,58]. Our results showed that RFC1 depletion resulted in significant reduction in the recruitment of both ATAD5 and BAZ1B to damage sites (Supplementary Fig. 5h–j). These findings suggest that ATAD5 and BAZ1B are independently recruited to DNA repair sites through their interaction with PCNA.

https://doi.org/10.1038/s41467-024-55005-3

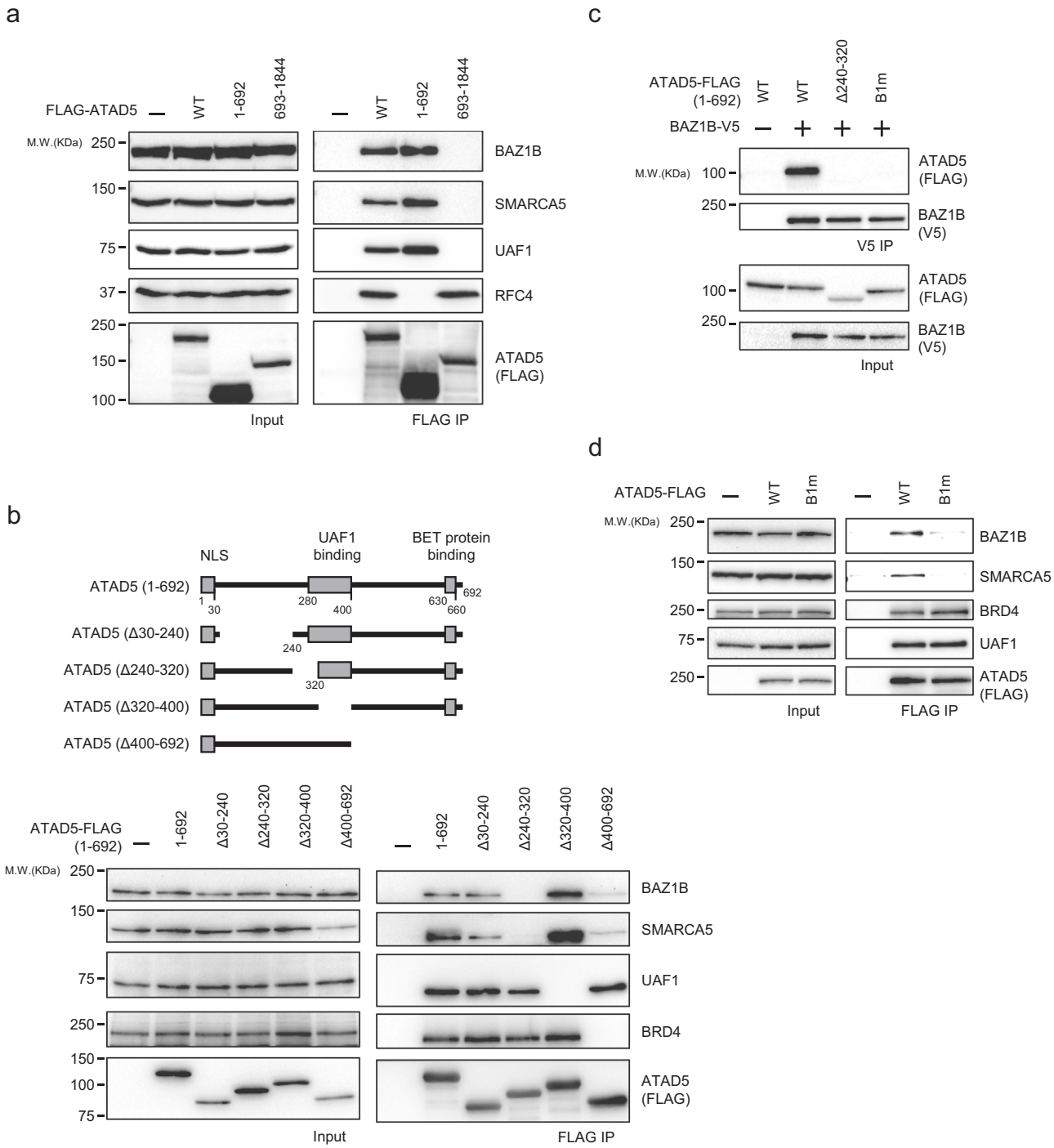

Fig. 2 | ATAD5 de-ubiquitination domain interacts with BAZ1B. a BAZ1B binds to the N-terminal domain of ATAD5. FLAG-tagged truncated mutants of ATAD5 were transiently expressed, followed by FLAG-immunoprecipitation. **b** The region of ATAD5 upstream UAF1-binding domain is important for BAZ1B binding. *Top*, Diagram illustrating ATAD5 (1–692) and its deletion variants. *Bottom*, the indicated FLAG-ATAD5 (1–692) variants were transiently expressed, and FLAG-immunoprecipitation was performed. **c**–**d** ATAD5 ^{264}TVSYEEF^{270} is crucial for its interaction with BAZ1B. The indicated FLAG-tagged variants of ATAD5 (1–692), (**c**), or full-length FLAG-tagged ATAD5 variants, (**d**), were transiently expressed, and FLAG-immunoprecipitation was performed. The ATAD5 B1m variant denotes a mutation that changes ^{264}TVSYEEF^{270} to AVAYAA (see Supplementary Fig. 2b). Source data are provided as a Source Data file.

Abrogation of the ATAD5-BAZ1B interaction causes premature de-ubiquitination of Ub-PCNA

Given that BAZ1B binds near the UAF1-binding motif of ATAD5 (Fig. 2), we hypothesized that interaction between ATAD5 and BAZ1B modulates the ATAD5 function in the de-ubiquitination of Ub-PCNA. To investigate whether this interaction influences Ub-PCNA de-ubiquitination, we analyzed the dynamics of PCNA mono-ubiquitination under oxidative stress. Treatment with hydrogen peroxide resulted in the accumulation of Ub-PCNA (Supplementary Fig. 6a). Following the removal of hydrogen peroxide, the level of Ub-PCNA returned to baseline within an hour. This dynamic response of PCNA ubiquitination following oxidative stress facilitates the exploration of the regulatory mechanisms behind Ub-PCNA de-ubiquitination.

https://doi.org/10.1038/s41467-024-55005-3

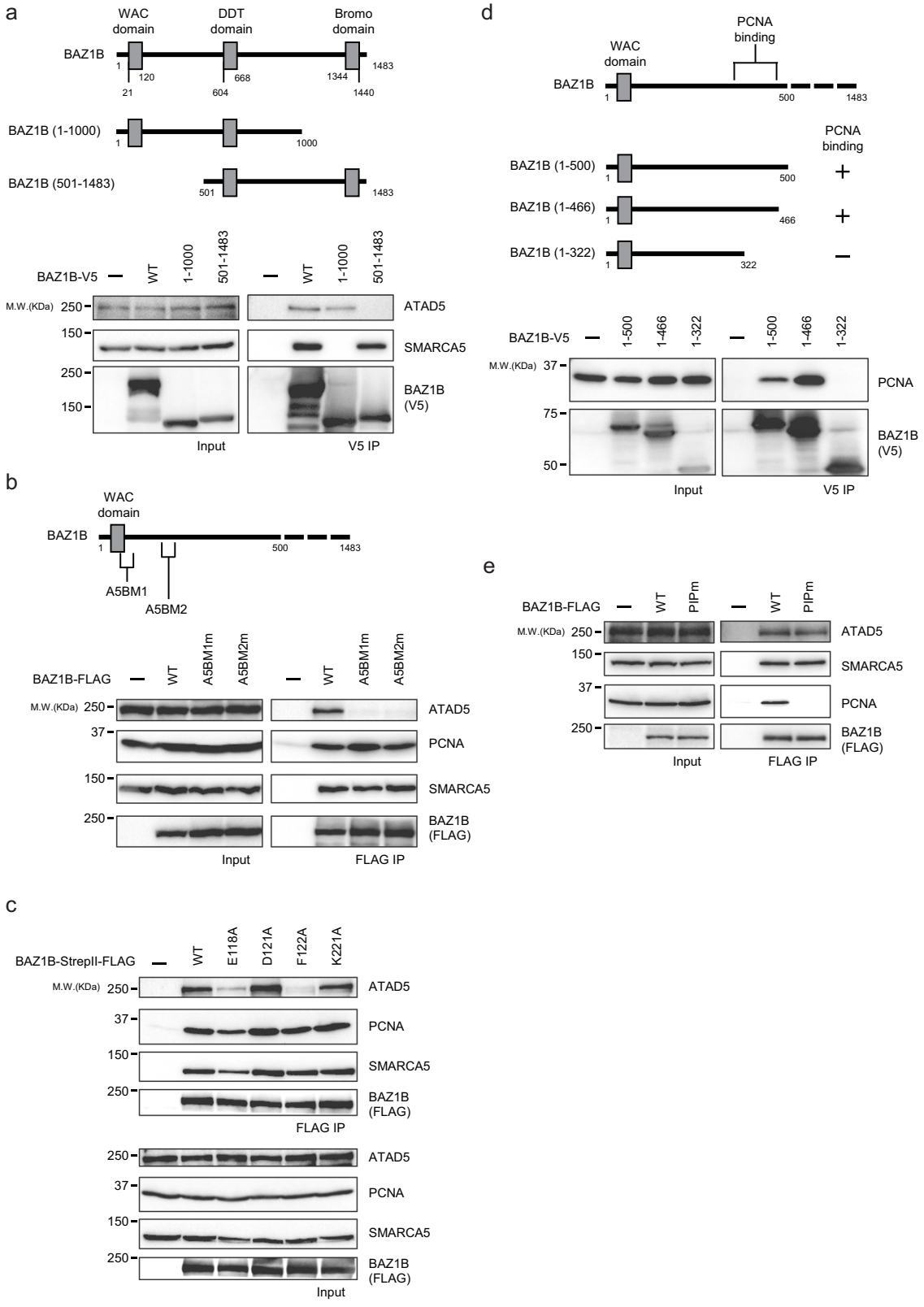

ATAD5 is essential for Ub-PCNA de-ubiquitination[26,55]. The knock-out of ATAD5 led to aberrant accumulation of Ub-PCNA and delayed de-ubiquitination after hydrogen peroxide treatment and subsequent removal (Supplementary Fig. 6b). In contrast, depletion of BAZ1B decreased Ub-PCNA levels after hydrogen peroxide treatment (Fig. 5a, Supplementary Fig. 6c), while SMARCA5 depletion did not decrease, but rather slightly increased Ub-PCNA levels. These findings suggest that BAZ1B has an opposing role to ATAD5 regarding Ub-PCNA levels. Importantly, BAZ1B depletion did not alter the level of PCNA on chromatin (Supplementary Fig. 6d).

To further investigate the impact of BAZ1B on PCNA cycling during DNA replication, we employed the isolated proteins on nascent DNA (iPOND) technique (Supplementary Fig. 6e) and found that BAZ1B depletion did not change the amounts of PCNA at replication forks.

Fig. 3 | BAZ1B N-terminal domains bind to ATAD5 and PCNA. a ATAD5 binds to the N-terminal domain of BAZ1B. *Top*, Diagram of BAZ1B variants analyzed for their interaction with ATAD5. *Bottom*, the indicated BAZ1B-V5 fragments were transiently expressed, followed by V5-immunoprecipitation. SMARCA5 bound to BAZ1B (501–1483), but ATAD5 did not. **b** BAZ1B ^{118}EECDF^{122} (A5BM1) and ^{221}KYDVK^{225} (A5BM2) are important for ATAD5 interaction. *Top*, Diagram illustrating the ATAD5 binding motifs on BAZ1B (see Supplementary Fig. 3b). *Bottom*, the indicated CLIP-BAZ1B-StrepII-FLAG variants were transiently expressed, and FLAG-immunoprecipitation was performed. A5BM1m and A5BM2m denote mutations where ^{18}EECDF^{122} is changed to AAAAA and ^{221}KYDVK^{225} is changed to AAAAA, respectively. **c** F122 in A5BM1 is crucial for ATAD5 interaction. The CLIP-BAZ1B-StrepII-FLAG variants containing single amino acid mutations in A5BM1 were transiently expressed, followed by FLAG-immunoprecipitation. **d** PCNA binds to BAZ1B (323–466). *Top*, Diagram of BAZ1B variants analyzed for their interaction with PCNA. *Bottom*, the indicated BAZ1B-V5 fragments were transiently expressed, and V5-immunoprecipitation was performed. **e** BAZ1B binds to PCNA and ATAD5 independently. Wild-type or PIPm (^{436}KQMTL^{440} changed to AAGAG) CLIP-BAZ1B-StrepII-FLAG variant were transiently expressed, and FLAG-immunoprecipitation was performed. The PIPm mutation abolished PCNA binding but did not affect the interaction with ATAD5. Source data are provided as a Source Data file.

Collectively, these results suggest that BAZ1B regulates the Ub-PCNA de-ubiquitination activity of ATAD5 rather than its unloading function.

To gain deeper insight into the role of the ATAD5-BAZ1B interaction, we expressed the ATAD5 B1m mutant in ATAD5 knock-out 293 T cells (Fig. 5b, Supplementary Fig. 6f, g). Under unperturbed conditions, wild-type and ATAD5 B1m cells exhibited similar levels of chromatin-bound PCNA and Ub-PCNA (Fig. 5b). Notably, after hydrogen peroxide treatment, the Ub-PCNA level was significantly lower in ATAD5 B1m cells compared to wild-type cells (Fig. 5b). This decreased Ub-PCNA level in ATAD5 B1m cells suggests that Ub-PCNA is de-ubiquitinated more rapidly in the absence of the ATAD5-BAZ1B interaction. Since ATAD5 facilitates Ub-PCNA de-ubiquitination through the UAF1-USP1 complex, the effect of BAZ1B on de-ubiquitination may be reduced without USP1. Consistent with this notion, USP1 depletion resulted in comparable Ub-PCNA levels in both wild-type and ATAD5 B1m cells (Fig. 5c, Supplementary Fig. 6h), suggesting that BAZ1B regulates Ub-PCNA de-ubiquitination rather than its generation. Additionally, in ATAD5 B1m cells, depletion of BAZ1B did not further reduce Ub-PCNA levels (Supplementary Fig. 6i). Together, these results indicate that BAZ1B negatively regulates Ub-PCNA de-ubiquitination through its interaction with ATAD5.

The ATAD5-BAZ1B interaction modulates Ub-PCNA de-ubiquitination

To biochemically investigate how BAZ1B regulates Ub-PCNA de-ubiquitination by ATAD5, we purified ATAD5 (1–603) and the BAZ1B-SMARCA5 (Supplementary Fig. 7a). First, we examined the interaction between purified ATAD5 (1–603) and BAZ1B-SMARCA5 (Fig. 6a). The in vitro pull-down assay demonstrated that BAZ1B-SMARCA5 co-isolated with ATAD5 (1–603) but not with the B1m mutant, indicating a direct interaction between ATAD5 and BAZ1B-SMARCA5 through the BAZ1B-binding motif, which is located near the UAF1-binding motif. This configuration suggests that the ATAD5-BAZ1B interaction may hinder the binding of ATAD5 to the UAF1-USP1 complex. To test this hypothesis, we challenged the ATAD5-UAF1 interaction with increasing amounts of the BAZ1B-SMARCA5 complex (Fig. 6b). While UAF1 co-isolated with ATAD5 (1–603), the addition of BAZ1B-SMARCA5 reduced the amount of co-isolated UAF1 (Fig. 6b, Supplementary Fig. 7b, c). In contrast, the addition of the ATAD5 (1–603, B1m) did not hinder the interaction between UAF1 and ATAD5 (Fig. 6c, Supplementary Fig. 7d). These findings imply that BAZ1B regulates the ATAD5-UAF1 interaction.

Next, we conducted an in vitro Ub-PCNA de-ubiquitination assay with UAF1-USP1 complex, ATAD5 (1–603), and BAZ1B-SMARCA5 complex (Fig. 6d, Supplementary Fig. 7e). ATAD5 (1–603) significantly enhanced Ub-PCNA de-ubiquitination by the UAF1-USP1 complex, thereby supporting the role of ATAD5 in this process. Interestingly, the addition of BAZ1B-SMARCA5 complex inhibited Ub-PCNA de-ubiquitination by ATAD5 (1–603) and the UAF1-USP1 complex (Fig. 6d). In contrast, the addition of BAZ1B-SMARCA5 did not affect Ub-PCNA de-ubiquitination by ATAD5 (1–603, B1m), emphasizing the essential nature of the ATAD5-BAZ1B interaction for regulating Ub-PCNA de-ubiquitination. These in vitro results align with the effects observed from the ATAD5 B1m mutation in a cellular context (Fig. 5). Collectively, these findings suggest that the interaction between ATAD5 and BAZ1B-SMARCA5 complex interferes with the ability of ATAD5 to facilitate Ub-PCNA de-ubiquitination by the UAF1-USP1 complex.

ATAD5 B1m cells are more sensitive to hydrogen peroxide

To investigate how misregulated Ub-PCNA de-ubiquitination due to the B1m mutation affects genome integrity, we treated ATAD5 B1m cells with hydrogen peroxide and monitored DNA replication through EdU incorporation. Under unperturbed conditions, both wild-type ATAD5 and ATAD5 B1m cells showed no defects in cell cycle progression or DNA replication (Supplementary Fig. 8a, b). However, following hydrogen peroxide treatment, DNA replication was significantly more inhibited in ATAD5 B1m cells compared to wild-type ATAD5 cells (Fig. 7a, Supplementary Fig. 8b). Notably, DNA damage checkpoint signals were elevated in ATAD5 B1m cells relative to wild-type ATAD5 cells (Fig. 7b, Supplementary Fig. 8c). Consistent with previous experiments, Ub-PCNA levels were lower in ATAD5 B1m cells, whereas levels of phosphorylated CHK1 and CHK2 were higher compared to wild-type cells.

To further assess DNA break formation after hydrogen peroxide treatment, we performed an alkaline comet assay, which revealed increased tail moments in ATAD5 B1m cells compared to wild-type cells, indicating a greater number of breaks (Fig. 7c, Supplementary Fig. 8d). These findings suggest that premature de-ubiquitination of Ub-PCNA leads to the accumulation of DNA breaks and the activation of DNA damage checkpoints. Consequently, due to increased genome instability, ATAD5 B1m cells exhibited greater sensitivity to hydrogen peroxide (Fig. 7d). Additionally, we found that the depletion of BAZ1B also increased sensitivity to hydrogen peroxide (Supplementary Fig. 8e). These results indicate that BAZ1B modulates PCNA ubiquitination levels by inhibiting ATAD5-mediated Ub-PCNA de-ubiquitination, thereby coordinating Ub-PCNA de-ubiquitination with DNA repair processes.

Discussion

In this report, we uncovered an unexpected role for BAZ1B in DNA repair. We discovered that BAZ1B interacts with ATAD5, a core subunit of the PCNA-unloading complex, and found that the BAZ1B-SMARCA5 binds to the Ub-PCNA de-ubiquitination domain of ATAD5 to negatively regulate de-ubiquitination. This modulation of Ub-PCNA de-ubiquitination by BAZ1B is crucial for maintaining genomic integrity during hydrogen peroxide-induced replication stress.

Previous studies have suggested that BAZ1B-mediated chromatin remodeling is important for proper re-assembly of daughter chromatin[53]. BAZ1B is enriched at active replication forks through its interaction with PCNA, and BAZ1B depletion leads to an increase in heterochromatin markers[1,4,41]. Given that ATAD5 is part of the PCNA-unloading complex and that BAZ1B interacts with PCNA, the BAZ1B-SMARCA5 complex may influence PCNA cycling on replicating DNA by repositioning nascent nucleosomes to facilitate PCNA unloading. However, our findings indicate that the depletion of BAZ1B or disruption of the ATAD5-BAZ1B interaction does not affect PCNA

https://doi.org/10.1038/s41467-024-55005-3

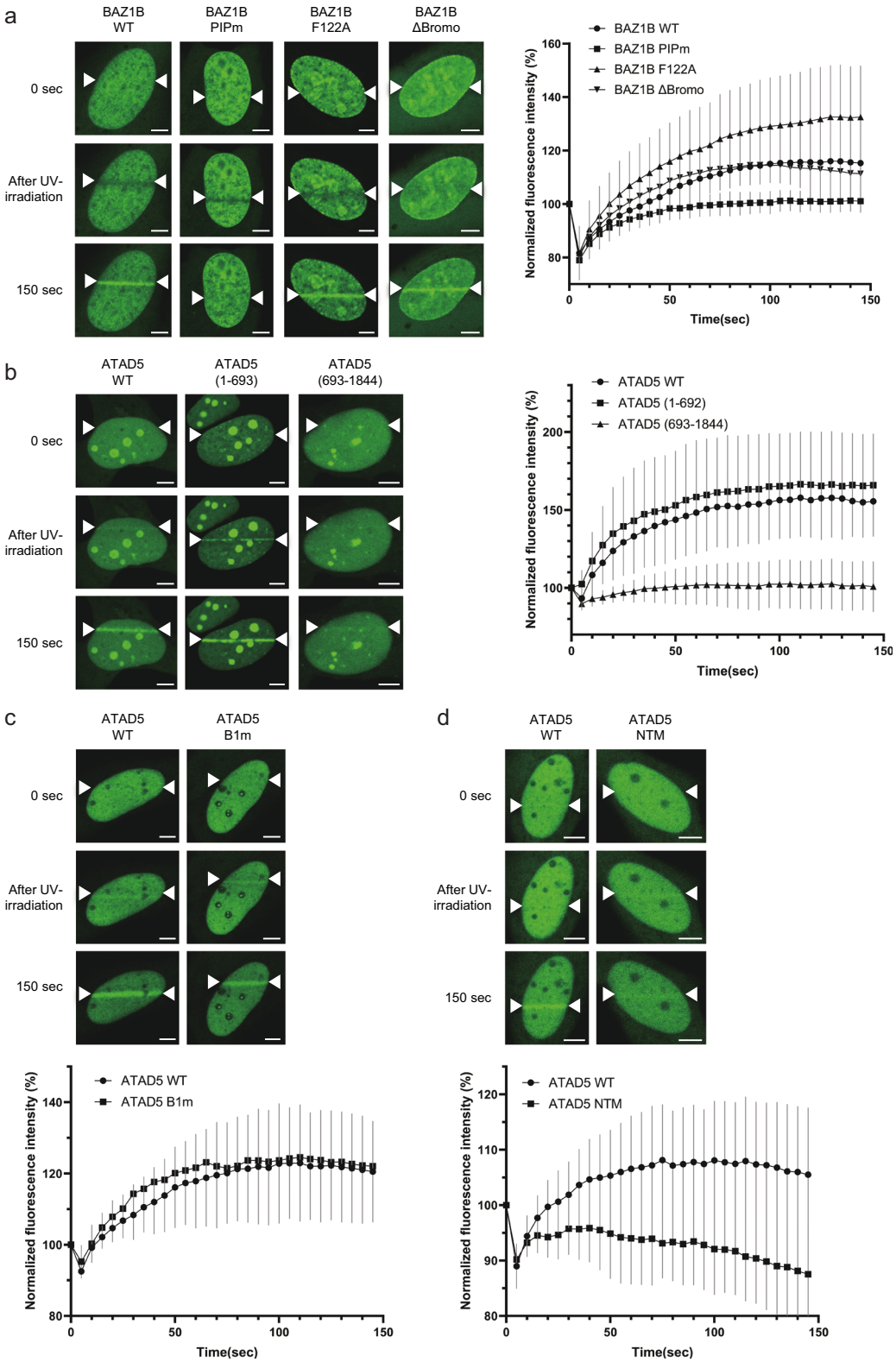

unloading (Fig. 5a, b, Supplementary Fig. 6c–e), suggesting that BAZ1B-SMARCA5-mediated daughter chromatin remodeling is not essential for this process. Instead, BAZ1B regulates PCNA ubiquitination levels through its interaction with ATAD5.

Upon hydrogen peroxide treatment, PCNA is loaded onto single-strand break sites to support polymerase δ-mediated repair synthesis[55]. Ub-PCNA can be generated due to polymerase stalling on damaged template DNA during repair synthesis. It has been suggested that redox stress modifies the replisome architecture and reduces replication fork speed during S phase[59], increasing transcription-replication conflicts and the likelihood of replication fork arrest[60,61]. We hypothesize that such replication fork stalling contributes to the accumulation of Ub-PCNA. Following the resolution of DNA lesions and the restoration of replication fork progression, timely de-ubiquitination of Ub-PCNA is necessary to turn off the lesion bypass signal and resume normal replication. Our data reveal that timely Ub-

Fig. 4 | BAZ1B and ATAD5 independently localize to DNA damage sites. a BAZ1B is recruited to micro-irradiated sites via PCNA. Indicated BAZ1B-FLAG-mNeonGreen variants were expressed in U2OS cells, which were then subjected to 355 nm UV laser micro-irradiation to the area indicated by the white arrowheads. The mean intensity of biological replicates ($n = 8$ for wild-type, $n = 6$ for PIPm, $n = 8$ for F122A and $n = 7$ for ΔBromo) are depicted as points, while the bands represent the standard deviation of all data points. **b** The N-terminal domain of ATAD5 is recruited to DNA damage sites. The indicated mNeonGreen-ATAD5 variants were expressed in U2OS cells, which were then subjected to 355 nm UV laser micro-irradiation to the area indicated by the white arrowheads. The mean intensity of biological replicates ($n = 7$ for wild-type, $n = 8$ for ATAD5 (1–692), and $n = 12$ for ATAD5 (693–1844)) are depicted as points, while the bands represent the standard deviation of all data points. **c** The interaction between ATAD5 and BAZ1B is not essential for the recruitment of ATAD5 to damage sites. Wild-type or B1m ATAD5-FLAG-mNeonGreen was expressed in U2OS cells, which were then subjected to 355 nm UV laser micro-irradiation to the area indicated by the white arrowheads. The mean intensity of biological replicates ($n = 6$ for wild-type and $n = 6$ for B1m) are depicted as points, while the bands represent the standard deviation of all data points. **d** The N-terminal region of ATAD5 is important for damage-site recruitment. Wild-type or NTM ATAD5-FLAG-mNeonGreen was expressed in U2OS cells, which were then subjected to 355 nm UV laser micro-irradiation to the area indicated by the white arrowheads. The mean intensity of biological replicates ($n = 9$ for wild-type and $n = 7$ for NTM) are depicted as points, while the bands represent the standard deviation of all data points. Refer to Supplementary Fig. 5d for the information on NTM. The scale bar in representative micrographs of (**a**–**d**) is 5 μm. Source data are provided as a Source Data file.

PCNA de-ubiquitination is achieved by the coordinated actions of two protein complexes: the BAZ1B-SMARCA5 complex and the ATAD5-RLC. ATAD5, in concert with the UAF1-USP1 complex, de-ubiquitinates Ub-PCNA at the final stage of DNA repair synthesis. In contrast, the BAZ1B-SMARCA5 complex may facilitate repair synthesis under replication stress conditions. Several studies highlighted BAZ1B's positive roles in DNA damage recovery and the restoration of transcription following DNA repair[49,62]. Our findings demonstrate that BAZ1B inhibits premature Ub-PCNA de-ubiquitination by the ATAD5-UAF1-USP1 complex. Because the BAZ1B binding site on ATAD5 is located near the UAF1 binding site, ATAD5-BAZ1B interaction may sterically hinder or alter the ATAD5-UAF1 interaction. Supporting this hypothesis, our in vitro studies show that BAZ1B interferes with the ATAD5-UAF1 association. Notably, ATAD5 is recruited to DNA damage sites independently of BAZ1B, suggesting that their interaction is not constitutive. Additionally, we did not observe an increase in the interaction between ATAD5 B1m and UAF1 in the immunoprecipitation assay, implying that BAZ1B regulates the ATAD5-UAF1 interaction locally at sites of replication stress. The proper association of UAF1-USP1 complex to ATAD5 is crucial for the de-ubiquitination of Ub-PCNA; any alterations in this interaction by BAZ1B may inhibit the de-ubiquitination. The interactions among ATAD5, BAZ1B, and PCNA appear to be dynamic throughout the DNA lesion bypass process. Notably, SMARCA5 depletion resulted in a slight increase in Ub-PCNA levels, in contrast to BAZ1B depletion, which decreased Ub-PCNA levels. This suggests that the interaction between BAZ1B and SMARCA5, or the chromatin remodeling activity of SMARCA5, may influence the dynamics of ATAD5 and BAZ1B during the de-ubiquitination of Ub-PCNA in the lesion bypass process. Further investigation will help elucidate the role of SMARCA5 in DNA lesion bypass. Recent reports suggest that USP1-mediated de-ubiquitination of Ub-PCNA promotes single-stranded DNA gap formation under replication stress[63]. De-ubiquitination of Ub-PCNA inhibits trans-lesion synthesis and causes nucleolytic degradation of nascent DNA. In ATAD5 B1m cells, unregulated USP1 activity may lead to increased single-stranded DNA gaps through this mechanism.

Upon exposure to UV, USP1 is degraded, promoting the accumulation of ubiquitinated PCNA[64]. We found that BAZ1B facilitates DNA repair synthesis by preventing premature Ub-PCNA de-ubiquitination. Our results demonstrate an additional layer of regulation of Ub-PCNA dynamics at DNA repair sites.

Methods

Cell lines and cell culture

Human embryonic kidney (HEK) 293 T cells (ATCC® CRL-3216™), HEK293T AD cells, U2OS cells (ATCC® HTB-96™), all purchased from the American Type Culture Collection (ATCC, Manassas, VA)), along with HeLa-PCNA^{GFP} [26] and HeLa-ATAD5^{mNeonGreen} [58] cells, were cultured in Dulbecco's modified Eagle's medium (Hyclone) supplemented with 10% fetal bovine serum (Merck) and 1% penicillin-streptomycin (Gibco). Cultures were maintained at 37 °C in a 5 % CO_2 atmosphere. To generate cell lines expressing HeLa-BAZ1B^{mNeonGreen} in a doxycycline-inducible manner, FRT-TO-mNeonGreen-BAZ1B cDNA was cloned and stably transfected into a HeLa Flp-in cell line. To induce BAZ1B^{mNeonGreen} expression, cells were treated with 100 ng/ml doxycycline and incubated for 48 h before analysis.

Transfections and RNA interference

Transfections of plasmid DNA and siRNAs were conducted using Transporter 5® Transfection Reagent (Polysciences), X-tremeGene HP DNA Transfection Reagent (Roche), and Lipofectamine RNAiMAX Transfection Reagent (Invitrogen), according to the manufacturer's protocols. Following transfection, the reagent was removed after 24 h, and fresh media were added. Transfected cells were harvested 48 h post-transfection for subsequent analyses.

Immunoprecipitation and western blot analysis

Whole-cell lysates were prepared by lysing cells in Buffer X (100 mM Tris-HCl [pH 8.5], 250 mM NaCl, 1 mM EDTA, 1 % NP40, and 5 mM $MgCl_2$) supplemented with cOmplete Protease Inhibitor Cocktail (Roche), phosphatase inhibitor PhosSTOP (Roche), and 50 U of Benzonase for 1 h at 4 °C. Lysates were cleared by centrifugation at 13,000 × *g* for 25 min at 4 °C. Protein concentrations were determined using the Bradford Assay (Bio-Rad). StrepII-tagged ATAD5 proteins were incubated with Strep-Tactin Sepharose High Performance resin (Cytiva), FLAG-tagged BAZ1B and ATAD5 proteins with anti-FLAG M2 agarose affinity beads (Sigma), and V5-tagged BAZ1B and SMARCA5 with anti-V5 agarose affinity beads (Sigma) for 1 h at 4 °C with constant rotation. Beads were washed three times with Buffer X. Strep-Tactin Sepharose bound proteins were eluted with Buffer X containing 5 mM *d*-Desthiobiotin, and anti-FLAG bead-bound proteins were eluted with Buffer X containing 0.15 mg/ml 3xFLAG peptide. Anti-V5 bead-bound proteins were resuspended in 1.5x SDS loading buffer and boiled at 100 °C for 5 min.

For endogenous BAZ1B immunoprecipitation, 2×10^7 HEK293T cells were lysed in Buffer X. Cleared lysates were incubated with rabbit IgG (Cell Signaling) or anti-BAZ1B antibody (Abcam) for 1 h at 4 °C, followed by the addition of Protein G Sepharose (Cytiva) for 4 h at 4 °C. Protein G Sepharose-bound antibodies were resuspended in 1.5x SDS loading buffer and boiled at 100 °C for 5 min.

Co-immunoprecipitated proteins were separated by SDS-PAGE, transferred to a nitrocellulose membrane, and analyzed by immunoblotting. Membranes were blocked in Tris-buffered saline containing 0.1% Tween® 20 supplemented with 5% skim milk powder. After incubation with primary antibodies in Tris-buffered saline containing 0.1% Tween® 20, proteins were visualized using secondary horseradish peroxidase-conjugated antibodies (Enzo Life Sciences) and Chemiluminescent Substrate (Thermo Fisher Scientific). Protein signals were captured using a ChemiDoc MP imaging system (Bio-Rad), and band intensities were quantified with Image Lab software version 5.2.1 (Bio-Rad).

https://doi.org/10.1038/s41467-024-55005-3

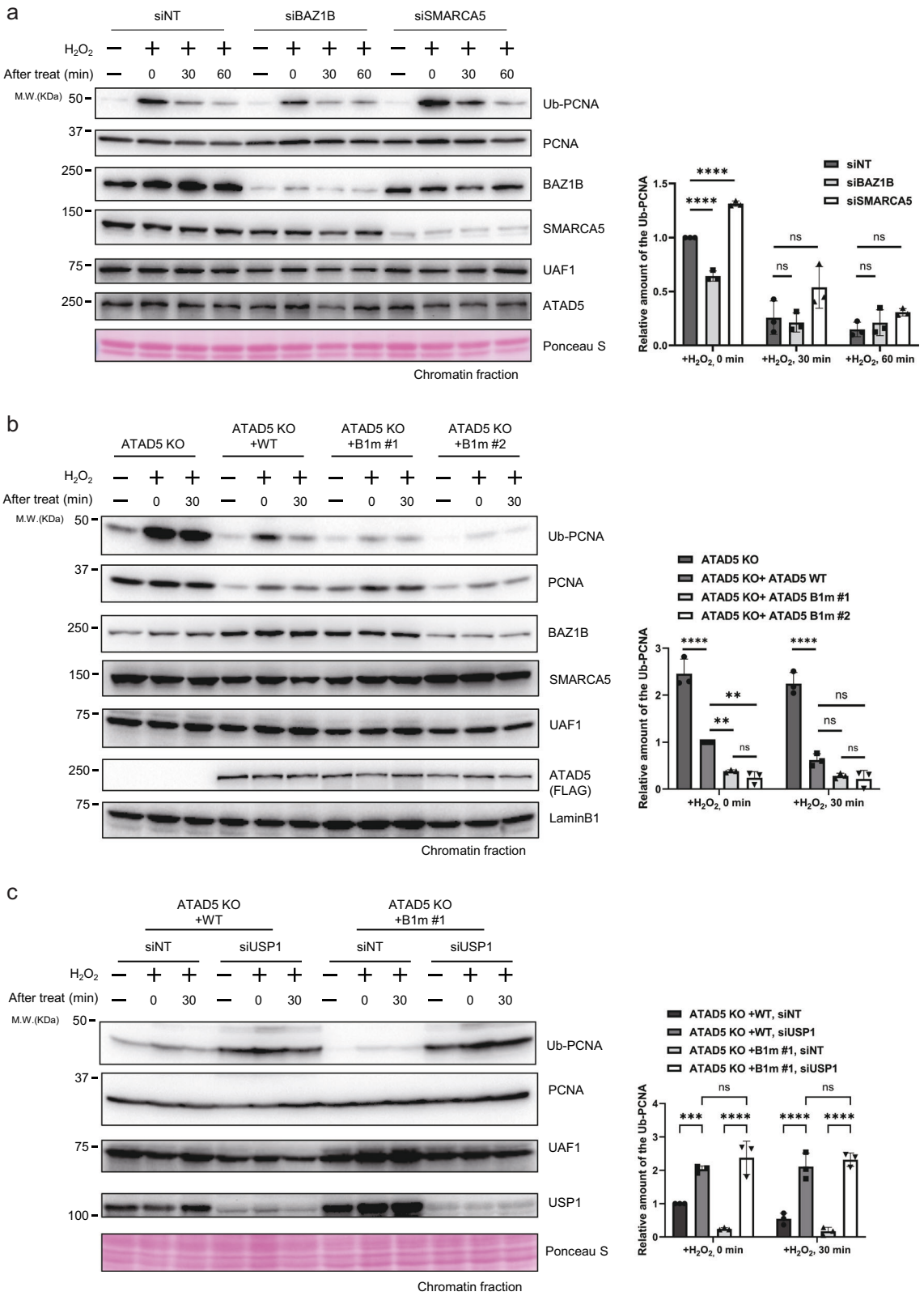

AP-MS analysis

For liquid chromatography with tandem mass spectrometry (LC-MS/MS), CLIP-ATAD5-StrepII-FLAG-encoded 293 T AD cells and 293 T cells transiently expressing BAZ1B-FLAG were immunoprecipitated using Strep-Tactin beads or anti-FLAG beads, respectively. Co-isolated interactors were separated by SDS-PAGE and subsequently visualized using Coomassie blue staining. The protein bands were excised into 10 mm sections and subjected to in-gel digestion with trypsin.

The resulting tryptic digests were analyzed through online reversed-phase chromatography on a Thermo Scientific Eazy nano LC 1200 UHPLC system, equipped with an autosampler. This analysis utilized an Acclaim PepMap™ 100 reversed-phase peptide trap column

Fig. 5 | BAZ1B regulates Ub-PCNA de-ubiquitination through ATAD5 interaction. a BAZ1B depletion decreases Ub-PCNA levels after H_2O_2 treatment. BAZ1B or SMARCA5 was depleted, and cells were treated with 1 mM H_2O_2 for 20 min. Following incubation in fresh media for the indicated times, chromatin fractions were prepared and analyzed by immunoblotting. The right panel shows the quantified relative amount of Ub-PCNA. Error bars represent the standard deviation of the mean from three independent replicates. Statistical analysis: Ordinary one-way ANOVA; $^{****}P \le 0.0001$ and ns: not significant. **b** Abrogation of the ATAD5-BAZ1B interaction reduces Ub-PCNA levels after oxidative stress. ATAD5 knock-out cells expressing either wild-type ATAD5 or ATAD5 B1m were treated with 0.3 mM H_2O_2 for 20 min. After incubating in fresh media for the indicated times, cells were harvested, and chromatin fractions were prepared. The right panel shows the quantified relative amount of Ub-PCNA. Error bars represent the standard deviation of the mean from three independent replicates. Statistical analysis: Ordinary one-way ANOVA; $^{****}P \le 0.0001$, $^{**}P \le 0.01$, and ns: not significant. **c** BAZ1B regulates Ub-PCNA de-ubiquitination by USP1. Cells with USP1 depletion, expressing either wild-type ATAD5 or ATAD5 B1m, were treated with 0.3 mM H_2O_2 for 20 min. Following incubation in fresh media for the indicated times, chromatin fractions were prepared and analyzed by immunoblotting. The right panel shows the quantified relative amount of Ub-PCNA. Error bars represent the standard deviation of the mean from three independent replicates. Statistical analysis: Two-way ANOVA; $^{****}P \le 0.0001$, $^{***}P \le 0.001$, and ns: not significant. Source data are provided as a Source Data file.

(75 µm inner diameter, 2 cm length) and a PepMap™ RSLC C18 analytical column (75 µm inner diameter, 15 cm length, 3 µm particle size), both sourced from Thermo Scientific. Electrospray ionization was performed at a flow rate of 300 nl/min.

The chromatography system was coupled in line with an Orbitrap Fusion Lumos mass spectrometer. Acquired spectra were searched against the UniProt human database using Proteome Discoverer 2.1 software with the Sequest-based search algorithm. Comparative analysis of the proteins identified in this study was conducted using Scaffold 4 Q + S.

Plasmids and small interfering RNAs siRNAs

Plasmids expressing full-length wild-type BAZ1B, SMARCA5, ATAD5, and their mutants were cloned into the pcDNA5™/FRT/TO plasmid (Thermo Fisher Scientific). The wild-type and mutant BAZ1B constructs (PIPm, F122A, and ΔBromo) were cloned to express N-terminal mNeonGreen tagged BAZ1B. Similarly, wild-type and mutant ATAD5 constructs (B1m, NTM, 1–692, 1–692 UAF1m, 1–400, and 693–1844) were cloned to express C-terminal mNeonGreen tagged ATAD5. Site-directed mutagenesis was performed using the QuikChange site-directed mutagenesis kit (Agilent Technologies), following the manufacturer's instructions. All constructs were verified by sequencing.

The siRNAs targeting the 3′ untranslated region (UTR) of ATAD5 mRNA were designed with sequences 5′-GGAAGGUAGAGUUCAUUAAUU-3′ (sense) and 5′-UUCCUUCCAUCUCAAGUAAUU-3′ (antisense). BAZ1B siRNAs were used with sequences 5′-AAGCCCGCUUGGAAAGGUACA-3′ (sense) and 5′-UGUACCUUUCCAAGCGGGCUU-3′ (antisense), and BAZ1B siRNAs #2 with sequences 5′-GGAGAUAGUUCGAUACUUUAU-3′ (sense) and 5′-AUAAAGUAUCGAACUAUCUCC-3′ (antisense). SMARCA5 siRNAs included sequences 5′-GUUCUUUCCUCCACGUUUA-3′ (sense) and 5′-UAAACGUGGAGGAAAGAAC-3′ (antisense). USP1 siRNAs had sequences 5′-AGCUACAAGUGAUACAUUA-3′ (sense) and 5′- UAAUGUAUCACUUGUAGCU-3′ (antisense). CKIIα siRNAs were designed with sequence 5′-GAUGACUACCAGCUGGUUC-3′ (sense) and 5′-GAACCAGCUGGUAGUCAUC-3′ (antisense). CKIIα′ siRNAs had sequence 5′-CAGUCUGAGGAGCCGCGAG-3′ (sense) and 5′-CUCGCGGCUCCUCAGACUG-3′ (antisense). All siRNAs were synthesized by Bioneer (South Korea). A nontargeting control siRNA (AccuTarget Negative Control siRNA) was also purchased from Bioneer (South Korea).

Chromatin fractionation

Cells were lysed in Buffer A (100 mM NaCl, 300 mM sucrose, 3 mM $MgCl_2$, 10 mM PIPES [pH 6.8], 1 mM EGTA, and 0.2% Triton X-100) supplemented with phosphatase inhibitor PhosSTOP and cOmplete Protease Inhibitor Cocktail (both from Roche), for 8 min on ice. Crude lysates were centrifuged at 5000 × *g* for 5 min at 4 °C to separate the chromatin-containing pellet from the soluble fraction. The pellet was washed once with phosphate-buffered saline (Sigma) and digested with 50 units of Benzonase (Enzynomics) for 60 min in RIPA Buffer (150 mM NaCl, 5 mM $MgCl_2$, 50 mM Tris–HCl pH 8.0, 5 mM EDTA, 1% Triton X-100, 0.1% SDS, and 0.5% sodium deoxycholate) containing phosphatase inhibitor PhosSTOP and cOmplete Protease Inhibitor Cocktail to extract chromatin-bound proteins. The chromatin-containing fractions were clarified by centrifugation at 13,000 × *g* for 25 min at 4 °C to remove debris. Protein concentrations were determined using the Bradford Assay (Bio-Rad), and proteins were analyzed by immunoblotting.

iPOND

iPOND was performed as described by Sirbu et al. (2011), with slight modifications[2]. Briefly, HEK293T cells were pulsed with 10 µM EdU (Life Technologies) for 20 min. EdU-labeled cells were then washed with a medium containing 10 µM thymidine to remove EdU, followed by a thymidine chase using the same medium for 0, 10, or 30 min. Cells were cross-linked with 1 % formaldehyde for 20 min at room temperature, quenched with 0.125 M glycine, and washed with phosphate-buffered saline (PBS) (Sigma). For the conjugation of EdU with biotin azide, cells were permeabilized with PBS containing 0.25 % Triton X-100 and incubated in click reaction buffer (10 mM sodium-L-ascorbate, 20 µM biotin azide (Life Technologies), and 2 mM $CuSO_4$) for 30 min at room temperature. After centrifugation, pellets were washed once with PBS containing 0.5 % BSA and twice with PBS. Cells were then resuspended in the lysis buffer (50 mM Tris-HCl [pH 8.0], and 1 % SDS) supplemented with protease inhibitors and sonicated. The lysates were cleared and incubated with streptavidin-agarose beads (Novagen) overnight at 4 °C. The beads were washed once with the lysis buffer, once with 1 M NaCl, and twice with lysis buffer. To elute proteins bound to nascent DNA, 2x SDS Laemmli sample buffer was added to the packed beads (1:1 v/v). Samples were incubated at 95 °C for 30 min, separated by SDS-PAGE, and analyzed by immunoblotting.

Protein purification

Proteins for in vitro PCNA mono-ubiquitination were purified as described previously[28]. The $RFC1^{\Delta N554}$-RFC was used due to its sufficiency in vitro PCNA loading assay[65]. Most proteins were purified using the Bac-to-Bac Baculovirus expression system (Thermo Fisher Scientific). Viruses were prepared using Sf9 cells, and protein expression was performed in Hi-5 cells (both from Thermo Fisher Scientific). For purification of Single polypeptide PCNA (3xPCNA), a construct expressing 3xPCNA with an N-terminal 10xHIS and C-terminal HSV and 3xFLAG tags was cloned into the pFastBac1 vector. For the UAF1-USP1 complex, N-terminal 10xHIS-tagged UAF1 and N-terminal 2xStrepII-tagged USP1 were cloned into the pFL multi-gene expression vector and expressed from a single construct. For the BAZ1B-SMARCA5 complex, N-terminal 2xStrepII- and C-terminal 3xFLAG-tagged BAZ1B, along with N-terminal 10xHis-tagged SMARCA5, were similarly cloned and expressed from a single construct. To purify proteins from insect cells, cells were lysed by sonication using a lysis buffer of 0.3 M potassium acetate in Buffer H (25 mM HEPES [pH 7.5], 1 mM EDTA, 1 mM EGTA, 2.5 mM magnesium acetate, 10 % glycerol, 1 mM DTT, and 0.02 % NP40), supplemented with cOmplete Protease Inhibitor Cocktail (Roche). Lysates were clarified by centrifugation at 36,000 × *g* for 2 h at 4 °C, and proteins were purified using anti-FLAG M2 agarose

https://doi.org/10.1038/s41467-024-55005-3

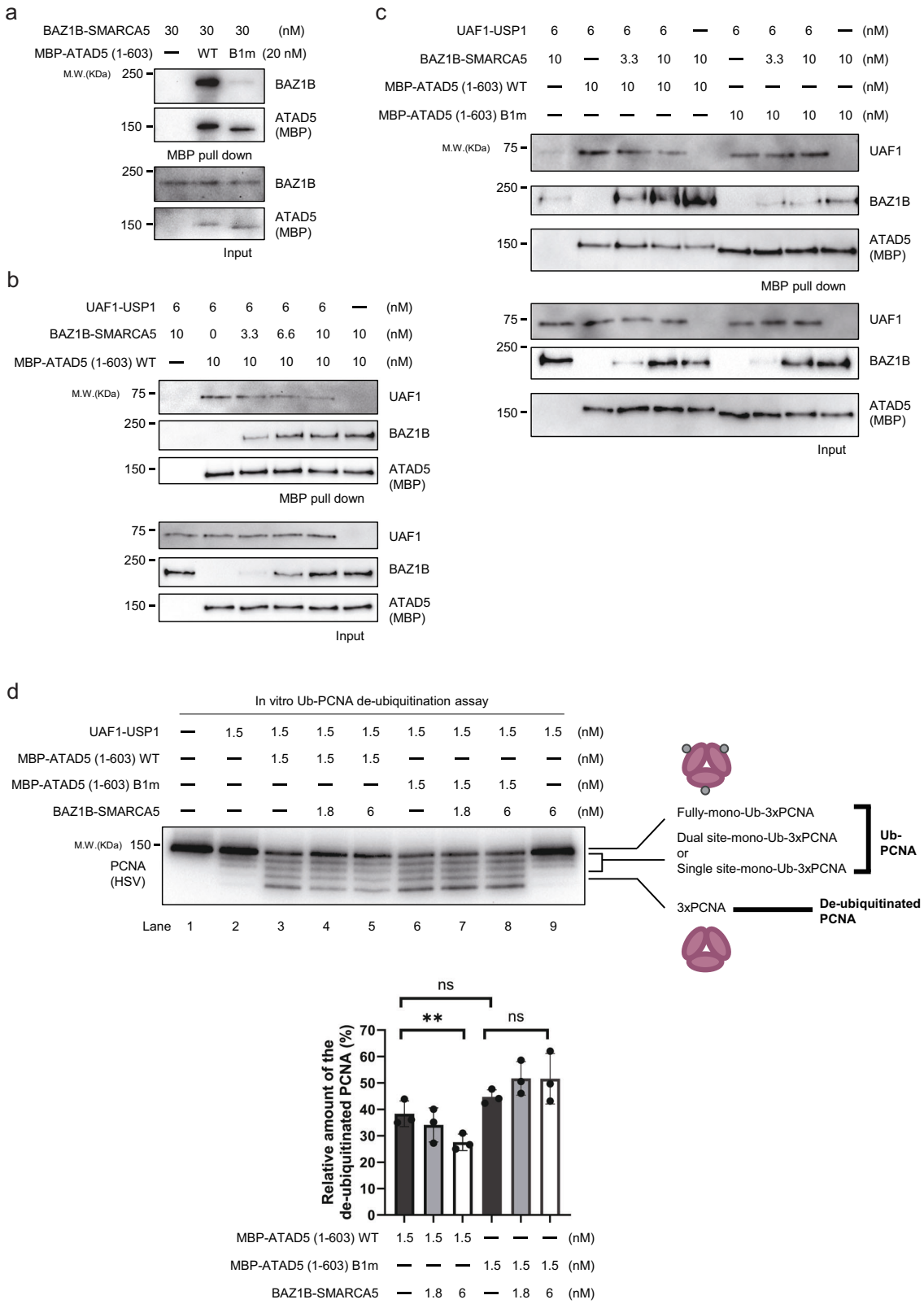

Fig. 6 | BAZ1B-SMARCA5 interferes with Ub-PCNA de-ubiquitination in vitro. **a** ATAD5 (1–603) interacts with BAZ1B-SMARCA5 in vitro. MBP-tagged ATAD5 (1–603) (20 nM) and various amounts of BAZ1B-SMARCA5 were mixed, and MBP-ATAD5 (1–603) was isolated using amylose resin. **b**–**c** BAZ1B-SMARCA5 interferes with the interaction between UAF1 and ATAD5. Wild-type, (**b**), or B1m MBP-ATAD5 (1–603), (**c**), were mixed with UAF1-USP1 and BAZ1B-SMARCA5, followed by amylose resin pull down. **d** BAZ1B-SMARCA5 inhibits Ub-PCNA de-ubiquitination by the ATAD5-UAF1-USP1 complex in vitro. A Ub-PCNA de-ubiquitination assay was performed using DNA-loaded Ub-PCNA and either wild-type or B1m MBP-ATAD5 (1–603) in the presence or absence of BAZ1B-SMARCA5. The bottom panel shows the quantified relative amounts of de-ubiquitinated PCNA. Error bars represent the standard deviation of the mean from three independent replicates. Statistical analysis: Two-way ANOVA; $^{**}P \leq 0.01$ and ns: not significant. Source data are provided as a Source Data file.

https://doi.org/10.1038/s41467-024-55005-3

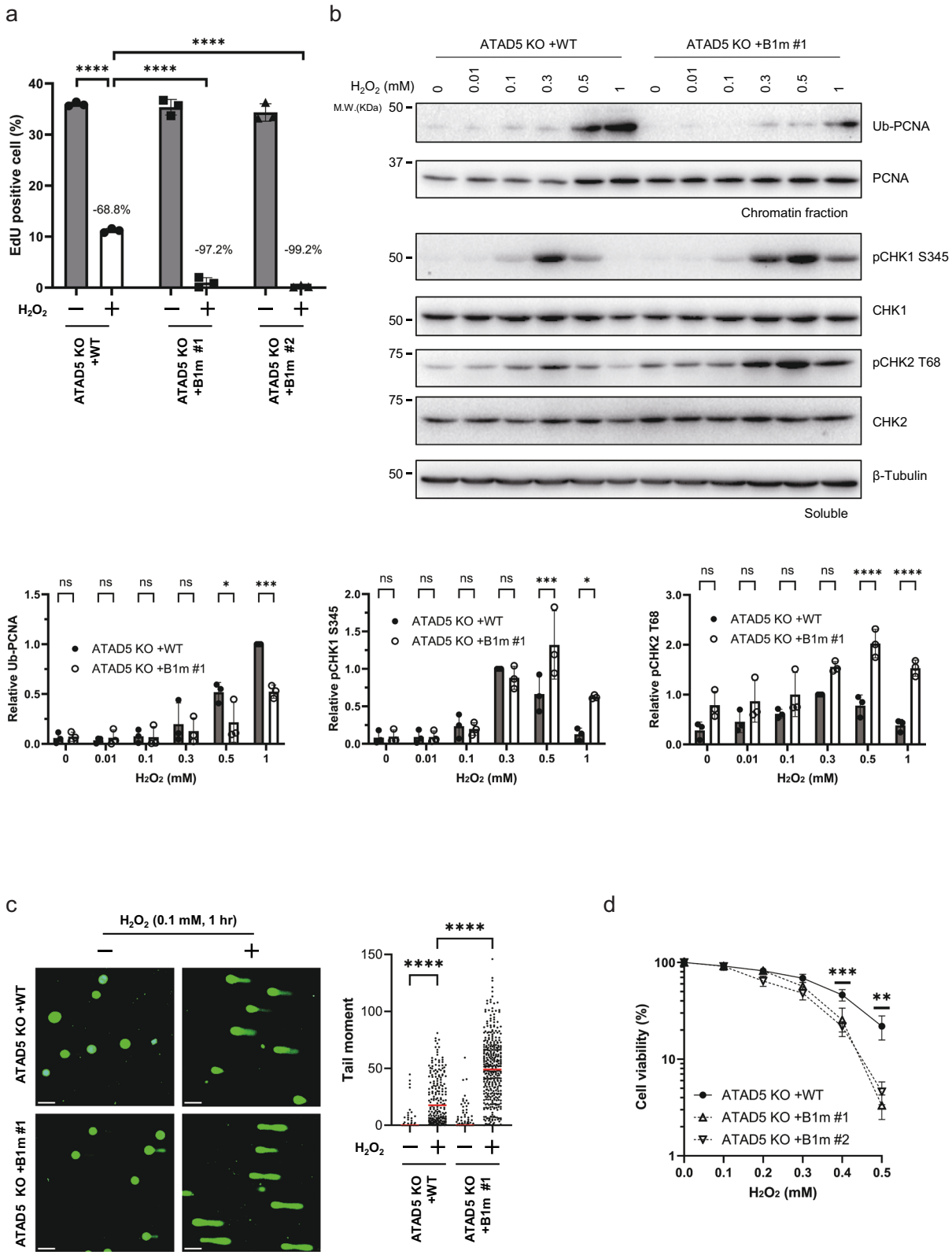

resin (Sigma) followed by ion exchange chromatography. For ATAD5 N-terminal fragments, the proteins were tagged with N-terminal MBP-2×StrepII and C-terminal 6×FLAG-S. These variants were expressed and purified from yeast strains. Yeast cells were grown in 2 L cultures to an O.D. = 0.8, and protein expression was induced by adding 2 % galactose for 6 h. Cells were harvested and re-suspended in one-third of the cell pellet volume using yeast lysis buffer (50 mM HEPES [pH 7.5], 1.5 M potassium glutamate, 0.8 M sorbitol, 10 mM magnesium acetate, 5% glycerol, and 0.02 % NP40) containing cOmplete Protease Inhibitor Cocktail. The cell suspension was frozen by dripping into liquid nitrogen and then ground into a powder using a Freezer-Mill 6870D (SPEX SamplePrep). Cleared lysates were obtained by centrifugation at 36,000 x *g* for 1 h at 4 °C after thawing. ATAD5 N-terminal fragments were purified using anti-FLAG M2 agarose resin (Sigma), followed by SP

Fig. 7 | ATAD5-BAZ1B interaction is important for maintaining genomic integrity. a DNA replication is more severely inhibited in ATAD5 B1m cells compared to wild-type under oxidative stress. Cells were labeled with EdU for 30 min and treated with H_2O_2 for 20 min as indicated. Following the Click reaction, EdU intensity was measured by flow cytometry. The relative decrease in the percentage of EdU-positive cells was calculated from three independent experiments. Error bars represent the standard deviation of the mean from three independent replicates. Statistical analysis: Two-way ANOVA; $^{****}P \le 0.0001$. **b** Phosphorylation of CHK1 and CHK2 increases in ATAD5 B1m cells after hydrogen peroxide treatment. The indicated cells were fractionated following treatment with hydrogen peroxide at the indicated concentration for 20 min. The bottom panel shows the quantified relative amounts of Ub-PCNA, phospho-CHK1, and phospho-CHK2. Error bars represent the standard deviation of the mean from three independent replicates. Statistical analysis: Two-way ANOVA; $^{****}P \le 0.0001$, $^{***}P \le 0.001$, $^{*}P \le 0.05$, and ns: not significant. **c** Abrogation of the ATAD5-BAZ1B interaction results in more DNA breaks after oxidative stress. An alkaline comet assay was performed on wild-type or B1m ATAD5 cells after treatment with 0.1 mM H_2O_2 for 1 h. The scale bar in representative micrographs is 100 μm. The right panel shows the quantification of the tail moment. At least 150 nuclei were quantified for each condition and red lines indicate the corresponding mean values. Statistical analysis: Two-way ANOVA; $^{****}P \le 0.0001$. **d** Abrogation of the ATAD5-BAZ1B interaction increases sensitivity to H_2O_2. A clonogenic survival assay was conducted with wild-type or B1m ATAD5 cells following treatment with H_2O_2 (0–0.5 mM for 16 h). Error bars represent the standard deviation of the mean from three independent replicates. Statistical analysis: Ordinary one-way ANOVA; $^{***}P \le 0.001$ and $^{**}P \le 0.01$. Source data are provided as a Source Data file.

Sepharose. The purified proteins were analyzed by SDS-PAGE followed by Coomassie blue staining. Proteins were aliquoted and stored at −80 °C.

355 nm UV-laser micro-irradiation

U2OS cells (4×10^4) were seeded in Lab-Tek Chambered Coverglasses (Thermo Fisher Scientific). After 24 h, fluorescence-tagged ATAD5 and BAZ1B DNA constructs were transfected using Transporter 5 (Polysciences). The cells were pre-incubated with 10 μM BrdU (Sigma) for 24 h prior to micro-irradiation, then switched to fresh media CO_2 Independent Medium (Gibco) supplemented with 10% FBS (Merck) and 2 mM L-Glutamine (Gibco) for 20 min before micro-irradiation. UV micro-irradiation was performed using a 355 nm diode laser at 100% power, which was projected through a C-Apochromat 40x/1.2 water immersion lens (488 nm argon laser) via a bleaching module (40 iterations) on an LSM880 confocal microscope (Carl Zeiss). The fluorescence intensity was analyzed using ZEN blue software (Carl Zeiss).

DNA substrates for de-ubiquitination reactions

130-mer DNA substrate was prepared as detailed in a previous report[28]. The annealed primer-template DNA was bound to streptavidin-coated magnetic beads (Dynabeads M-280, Invitrogen), and unbound DNA/oligonucleotides were washed away. The bead-attached DNA was resuspended in 0.3 M potassium acetate Buffer H without magnesium acetate. The substrate includes a TALE-binding sequence on the opposite side of biotinylation. For the PCNA-loading reaction, 2.5 pmol the DNA substrate was pre-incubated with 50 nM TALE in a 40 μL reaction mixture containing 25 mM HEPES [pH 7.5], 1 mM EDTA, 1 mM EGTA, 2.5 mM magnesium acetate, 10% glycerol, 300 mM potassium acetate, 1 mM ATP, 0.02 % NP40, and 1 mM DTT at 37 °C for 30 min prior to the reaction.

In vitro mono-Ub PCNA de-ubiquitination reactions

This method was performed as described previously, with minor modifications[28]. For the in vitro PCNA loading assay, two buffers were prepared: a standard 2x loading reaction buffer (50 mM HEPES [pH 7.5], 12 mM magnesium acetate, 0.1 mM zinc acetate, 1 mM DTT, 20 mM phosphocreatine, 6 mM ATP, 0.02% NP40, 10% glycerol, 0.4 mg/mL BSA, and 1x cOmplete Protease Inhibitor Cocktail (Roche)) and a protein dilution buffer (25 mM HEPES [pH 7.5], 1 mM EDTA, 1 mM EGTA, 2.5 mM magnesium acetate, 10% glycerol, 0.3 M potassium acetate, 1 mM DTT, and 0.02% NP40). Initially, 20 μL of 2x loading reaction buffer was mixed with 20 μL of protein mixture containing 25 nM RFC(RFC1$^{\Delta N554}$) and 500 nM 3xPCNA. The PCNA-loading reaction was performed by adding 40 μL of this mixture to bead-conjugated DNA substrate after TALE binding. The reaction mixture was incubated in a Thermomixer (Eppendorf) at 37 °C and 1200 rpm for 30 min. After the reaction, the remaining RFC and unbound PCNA were removed by washing the beads once with 0.3 M KCl Buffer H, once with 0.5 M KCl Buffer H, and then once more with 0.3 M KCl Buffer H.

For the mono-ubiquitination reaction, a standard 4x ubiquitination reaction buffer was prepared (80 mM HEPES [pH 7.5], 4 mM DTT, 40 mM $MgCl_2$, and 4 mM ATP). The mono-ubiquitination reaction mixture was prepared by combining 7.5 μL of the 4x ubiquitination reaction buffer with 22.5 μL of a protein mixture containing 50 nM UBA1, 100 nM RAD6B-RAD18 and 1.25 μM ubiquitin. Next, 30 μL of the mono-ubiquitination reaction mixture was added to the collected DNA beads with loaded 3xPCNA. After incubating the reaction mixture at 30 °C in a Thermomixer for 20 min, the reaction was terminated by washing with 0.3 M KCl Buffer H.

The de-ubiquitination reaction was performed using a standard 4x ubiquitination reaction buffer containing various concentrations of UAF1-USP1, ATAD5 (1–603), and BAZ1B-SMARCA5. Subsequently, 30 μL of the de-ubiquitination reaction mixture was added to the Ub-PCNA loaded DNA-beads and incubated for 20 min at 25 °C in a Thermomixer. Finally, the DNA beads were resuspended in 30 μL of digestion buffer (25 mM HEPES [pH 7.5], 1 mM EDTA, 1 mM EGTA, 5 mM magnesium acetate, 10 % glycerol, 1 mM DTT, 10 mM $MgCl_2$, and 1 mM ATP) containing 1 unit of DNase I (Promega).

In vitro pull-down assay

To assess the interaction between purified ATAD5 proteins and BAZ1B-SMARCA5 or UAF1-USP1, purified MBP-tagged ATAD5 (1–603) was mixed with varying concentrations of BAZ1B-SMARCA5 or UAF1-USP1 in 100 μL of 100 mM KCl Buffer H. The protein mixtures were incubated on ice for 1 h with Amylose resin (NEB) and then subjected to pull-down via centrifugation at 5000 x *g* for 5 min at 4 °C). The resin-bound ATAD5 (1–603) was eluted using 10 mM maltose in Buffer H. Isolated proteins were analyzed by SDS-PAGE followed by immunoblotting.

Alkaline COMET assay

The alkaline COMET assay was performed according to the instructions provided by CometAssay® (Trevigen). Briefly, cells were lysed using CometAssay Lysis Solution (R&D systems). The cell suspension was mixed with CometAssay LMAgarose (R&D systems) and then placed on the CometSlide (R&D systems). DNA was subsequently stained with SYBR Gold and visualized using a BX53 fluorescence microscope (Olympus). The DNA tail moment was calculated using TriTek CometScore software version 2.0.

Flow cytometry and EdU incorporation analysis

Cells were labeled with 10 mM EdU for 30 min prior to harvesting. For flow cytometry analysis, samples were prepared using the Click-iT™ Plus EdU Alexa Fluor™ 647 Flow Cytometry Assay Kit (Invitrogen) according to the manufacturer's instructions. Flow cytometry was conducted on a FACSVerse™ flow cytometer, and data were acquired

using BD FACSuite™ software (BD Biosciences). Data analysis was performed using FlowJo software (Tree Star).

Clonogenic survival assay

HEK293T AD wild-type ATAD5 cells and ATAD5 B1m cells were seeded onto 60-mm plates at a density of 6×10^2 cells and 3×10^2 cells per plate, respectively. Cells were treated with hydrogen peroxide for 16 h. For the BAZ1B siRNA experiments, HEK293T was seeded onto 60 mm plates at a density of 1×10^3 cells per plate. Transfection of BAZ1B siRNA was performed using Lipofectamine RNAiMAX Transfection Reagent (Invitrogen) according to the manufacturer's instructions. The transfection reagent was removed 24 h after the transfection, and cells were then treated with hydrogen peroxide for 16 h.

Following hydrogen peroxide treatment, the medium was discarded, and fresh medium was added for a recovery period of 5 days. Cells were then washed with PBS, fixed with 4% paraformaldehyde for 20 min, and stained with 1.5% methylene blue in 70% ethanol for 2 h.

Protein-protein interaction structure prediction for using Alphafold-Multimer

To investigate the interaction motifs in protein-protein interactions, we performed structure prediction using Alphafold-multimer[66,67]. Alphafold (v2.3.2) was installed on a local Ubuntu (v24.04 LTS) environment equipped with an RTX 4090 graphic card (24GB) and 64 GB of RAM. Amino acid sequence FASTA inputs were prepared for BAZ1B (UniProtKB: Q9UIG0, residues 1–500), ATAD5 (UniProtKB: Q96QE3, residues 1–603) and PCNA (UniProtKB: P12004), which were then paired as described. Default parameters were used, with the exception of max_template_date=2024-04-01. The top-ranked model with the highest confidence scores, as calculated by AlphaFold, was selected for further analysis in PyMol. All residues specified in the ATAD5-BAZ1B interaction motif exhibited pLDDT values greater than 90. The predicted structures were visualized by ChimeraX.

Reagents and antibodies

The following reagents were used in this study: hydrogen peroxide (Sigma, H1009), hydroxyurea (Sigma, H8627) and camptothecin (Sigma, C9911).

The following antibodies were used in this study: anti-BAZ1B (WSTF) antibody (Abcam, ab51256, 1:500), (Santa Cruz Biotechnology, sc-514287, 1:200), (Cell Signaling, #2152, 1:500); anti-UAF1 (WDR48) antibody (Santa Cruz Biotechnology, sc-514473, 1:100); anti-beta Tubulin antibody (Abcam, ab15568, 1:1000); anti-FLAG antibody (Sigma, F3165, 1:1000); anti-SMARCA5 (SNF2H) antibody (Abcam, ab3749, 1:1000); anti-GAPDH antibody (Santa Cruz Biotechnology, sc-32233, 1:1000); anti-Lamin B1 antibody (Abcam, ab16048, 1:1000); anti-V5 antibody (Sigma, V8137, 1:2000); anti-Histone H2A.X S139ph (γH2AX) antibody (GeneTex, GTX127340, 1:1000); anti-RFC4 antibody (Abcam, ab182145, 1:1000); anti-BRD4 antibody (Bethyl, A301-985A50, 1:1000); anti-PCNA antibody (Santa Cruz Biotechnology, sc-56, 1:2000) (Abcam, ab70472, 1:2000); anti-Ubiquityl-PCNA (Lys164) antibody (Cell Signaling, #13439, 1:1000); anti-USP1 antibody (Bethyl, A301-700A, 1:500); anti-MBP antibody (Santa Cruz Biotechnology, sc-13564, 1:200); anti-HSV antibody (Abcam, ab19355, 1:1000); anti-Phospho-CHK1 (Ser345) antibody (Cell Signaling, #2348, 1:1000); anti-CHK1 antibody (Cell Signaling, #2360, 1:1000); anti-Phospho-CHK2 (Thr68) antibody (Cell Signaling, #2197, 1:1000); anti-CHK2 antibody (Santa Cruz Biotechnology, sc-17747, 1:1000); anti-casein kinase IIα' antibody (Santa Cruz Biotechnology, sc-514403, 1:1000); anti-RFC1 (Santa Cruz Biotechnology, sc-271656, 1:100); anti-Histone H3 antibody (Merck, 07-690, 1:50000); anti-Histone H2A.X antibody (Cell Signaling, #2595, 1:1000); The anti-human ATAD5 antibody (1:1000) was raised in rabbits using the N-terminal 1–297 amino-acid fragment and then affinity-purified.

Statistics and reproducibility

Quantification of immunoblots was carried out using Bio-Rad Image Lab software. Statistical analyses were conducted using GraphPad Prism. Details of the statistical analysis for individual experiments are provided in the Figure legends and results section. Unless otherwise specified, all experiments were performed in triplicates, and representative experiments are shown. Bar graphs display the mean and standard deviation, with individual data points overlaid as scatter dot plots. Statistical significance is indicated as follows: ns = not significant, $^{*}P \le 0.05$, $^{**}P \le 0.01$, $^{***}P \le 0.001$, and $^{****}P \le 0.0001$. The exact p-value is shown in the Source Data file.

Reporting summary

Further information on research design is available in the Nature Portfolio Reporting Summary linked to this article.

Data availability

All the data can be found in either the main text or the supplementary materials. Source data are provided with this paper. The mass spectrometry proteomics data have been deposited to the ProteomeXchange with the dataset identifier PXD050108. Source data are provided with this paper.

References

1. Sirbu, B. M. et al. Identification of proteins at active, stalled, and collapsed replication forks using isolation of proteins on nascent DNA (iPOND) coupled with mass spectrometry. *J. Biol. Chem.* **288**, 31458–31467 (2013).
2. Sirbu, B. M. et al. Analysis of protein dynamics at active, stalled, and collapsed replication forks. *Genes Dev.* **25**, 1320–1327 (2011).
3. Aleksandrov, R. et al. Protein Dynamics in Complex DNA Lesions. *Mol. Cell* **69**, 1046–1061.e5 (2018).
4. Ribeyre, C. et al. Nascent DNA Proteomics Reveals a Chromatin Remodeler Required for Topoisomerase I Loading at Replication Forks. *Cell Rep.* **15**, 300–309 (2016).
5. Wessel, S. R., Mohni, K. N., Luzwick, J. W., Dungrawala, H. & Cortez, D. Functional Analysis of the Replication Fork Proteome Identifies BET Proteins as PCNA Regulators. *Cell Rep.* **28**, 3497–3509.e4 (2019).
6. Zhuang, Z. et al. Regulation of polymerase exchange between Poleta and Poldelta by monoubiquitination of PCNA and the movement of DNA polymerase holoenzyme. *Proc. Natl. Acad. Sci. USA* **105**, 5361–5366 (2008).
7. Wit, N. et al. Roles of PCNA ubiquitination and TLS polymerases kappa and eta in the bypass of methyl methanesulfonate-induced DNA damage. *Nucleic Acids Res.* **43**, 282–294 (2015).
8. Garg, P. & Burgers, P. M. Ubiquitinated proliferating cell nuclear antigen activates translesion DNA polymerases eta and REV1. *Proc. Natl. Acad. Sci. USA* **102**, 18361–18366 (2005).
9. Moldovan, G. L., Pfander, B. & Jentsch, S. PCNA, the maestro of the replication fork. *Cell* **129**, 665–679 (2007).
10. Krishna, T. S., Kong, X. P., Gary, S., Burgers, P. M. & Kuriyan, J. Crystal structure of the eukaryotic DNA polymerase processivity factor PCNA. *Cell* **79**, 1233–1243 (1994).
11. Tsurimoto, T. & Stillman, B. Replication factors required for SV40 DNA replication in vitro. I. DNA structure-specific recognition of a primer-template junction by eukaryotic DNA polymerases and their accessory proteins. *J. Biol. Chem.* **266**, 1950–1960 (1991).
12. Bowman, G. D., O'Donnell, M. & Kuriyan, J. Structural analysis of a eukaryotic sliding DNA clamp-clamp loader complex. *Nature* **429**, 724–730 (2004).
13. Fujisawa, R., Ohashi, E., Hirota, K. & Tsurimoto, T. Human CTF18-RFC clamp-loader complexed with non-synthesising DNA polymerase epsilon efficiently loads the PCNA sliding clamp. *Nucleic Acids Res.* **45**, 4550–4563 (2017).

14. Zhuang, Z., Yoder, B. L., Burgers, P. M. & Benkovic, S. J. The structure of a ring-opened proliferating cell nuclear antigen-replication factor C complex revealed by fluorescence energy transfer. *Proc. Natl. Acad. Sci. USA* **103**, 2546–2551 (2006).
15. Stodola, J. L. & Burgers, P. M. Resolving individual steps of Okazaki-fragment maturation at a millisecond timescale. *Nat. Struct. Mol. Biol.* **23**, 402–408 (2016).
16. Mondol, T., Stodola, J. L., Galletto, R. & Burgers, P. M. PCNA accelerates the nucleotide incorporation rate by DNA polymerase delta. *Nucleic Acids Res.* **47**, 1977–1986 (2019).
17. Watanabe, K. et al. Rad18 guides poleta to replication stalling sites through physical interaction and PCNA monoubiquitination. *EMBO J.* **23**, 3886–3896 (2004).
18. Hoege, C., Pfander, B., Moldovan, G. L., Pyrowolakis, G. & Jentsch, S. RAD6-dependent DNA repair is linked to modification of PCNA by ubiquitin and SUMO. *Nature* **419**, 135–141 (2002).
19. Davies, A. A., Huttner, D., Daigaku, Y., Chen, S. & Ulrich, H. D. Activation of ubiquitin-dependent DNA damage bypass is mediated by replication protein a. *Mol. Cell* **29**, 625–636 (2008).
20. Choe, K. N. & Moldovan, G. L. Forging Ahead through Darkness: PCNA, Still the Principal Conductor at the Replication Fork. *Mol. Cell* **65**, 380–392 (2017).
21. Mailand, N., Gibbs-Seymour, I. & Bekker-Jensen, S. Regulation of PCNA-protein interactions for genome stability. *Nat. Rev. Mol. Cell Biol.* **14**, 269–282 (2013).
22. McCulloch, S. D. & Kunkel, T. A. The fidelity of DNA synthesis by eukaryotic replicative and translesion synthesis polymerases. *Cell Res.* **18**, 148–161 (2008).
23. Brown, S., Niimi, A. & Lehmann, A. R. Ubiquitination and deubiquitination of PCNA in response to stalling of the replication fork. *Cell Cycle* **8**, 689–692 (2009).
24. Fox, J. T., Lee, K. Y. & Myung, K. Dynamic regulation of PCNA ubiquitylation/deubiquitylation. *FEBS Lett.* **585**, 2780–2785 (2011).
25. Alvarez, V. et al. PCNA Deubiquitylases Control DNA Damage Bypass at Replication Forks. *Cell Rep.* **29**, 1323–1335.e5 (2019).
26. Lee, K. Y., Fu, H., Aladjem, M. I. & Myung, K. ATAD5 regulates the lifespan of DNA replication factories by modulating PCNA level on the chromatin. *J. Cell Biol.* **200**, 31–44 (2013).
27. Ryu, E. et al. Distinct Motifs in ATAD5 C-Terminal Domain Modulate PCNA Unloading Process. *Cells* **11**, 1832 (2022).
28. Kang, M. S. et al. Regulation of PCNA cycling on replicating DNA by RFC and RFC-like complexes. *Nat. Commun.* **10**, 2420 (2019).
29. Miyata, T. et al. Open clamp structure in the clamp-loading complex visualized by electron microscopic image analysis. *Proc. Natl. Acad. Sci. USA* **102**, 13795–13800 (2005).
30. Bellaoui, M. et al. Elg1 forms an alternative RFC complex important for DNA replication and genome integrity. *EMBO J.* **22**, 4304–4313 (2003).
31. Kubota, T., Nishimura, K., Kanemaki, M. T. & Donaldson, A. D. The Elg1 replication factor C-like complex functions in PCNA unloading during DNA replication. *Mol. Cell* **50**, 273–280 (2013).
32. Lee, K. Y. et al. Human ELG1 regulates the level of ubiquitinated proliferating cell nuclear antigen (PCNA) through Its interactions with PCNA and USP1. *J. Biol. Chem.* **285**, 10362–10369 (2010).
33. Kang, M. S. et al. PCNA Unloading Is Negatively Regulated by BET Proteins. *Cell Rep.* **29**, 4632–4645.e5 (2019).
34. Ransom, M., Dennehey, B. K. & Tyler, J. K. Chaperoning histones during DNA replication and repair. *Cell* **140**, 183–195 (2010).
35. Liu, B., Yip, R. & Zhou, Z. Chromatin remodeling, DNA damage repair and aging. *Curr. Genomics* **13**, 533–547 (2012).
36. Gursoy-Yuzugullu, O., House, N. & Price, B. D. Patching Broken DNA: Nucleosome Dynamics and the Repair of DNA Breaks. *J. Mol. Biol.* **428**, 1846–1860 (2016).
37. Hauer, M. H. & Gasser, S. M. Chromatin and nucleosome dynamics in DNA damage and repair. *Genes Dev.* **31**, 2204–2221 (2017).
38. Stadler, J. & Richly, H. Regulation of DNA Repair Mechanisms: How the Chromatin Environment Regulates the DNA Damage Response. *Int J. Mol. Sci.* **18**, 1715 (2017).
39. Zhang, W., Feng, J. & Li, Q. The replisome guides nucleosome assembly during DNA replication. *Cell Biosci.* **10**, 37 (2020).
40. Harrod, A., Lane, K. A. & Downs, J. A. The role of the SWI/SNF chromatin remodelling complex in the response to DNA double strand breaks. *DNA Repair (Amst.)* **93**, 102919 (2020).
41. Poot, R. A. et al. The Williams syndrome transcription factor interacts with PCNA to target chromatin remodelling by ISWI to replication foci. *Nat. Cell Biol.* **6**, 1236–1244 (2004).
42. Bozhenok, L., Wade, P. A. & Varga-Weisz, P. WSTF-ISWI chromatin remodeling complex targets heterochromatic replication foci. *EMBO J.* **21**, 2231–2241 (2002).
43. Oppikofer, M. et al. Expansion of the ISWI chromatin remodeler family with new active complexes. *EMBO Rep.* **18**, 1697–1706 (2017).
44. Barnett, C. & Krebs, J. E. WSTF does it all: a multifunctional protein in transcription, repair, and replication. *Biochem Cell Biol.* **89**, 12–23 (2011).
45. Aydin, O. Z., Vermeulen, W. & Lans, H. ISWI chromatin remodeling complexes in the DNA damage response. *Cell Cycle* **13**, 3016–3025 (2014).
46. Vintermist, A. et al. The chromatin remodelling complex B-WICH changes the chromatin structure and recruits histone acetyltransferases to active rRNA genes. *PLoS One* **6**, e19184 (2011).
47. Percipalle, P. et al. The chromatin remodelling complex WSTF-SNF2h interacts with nuclear myosin 1 and has a role in RNA polymerase I transcription. *EMBO Rep.* **7**, 525–530 (2006).
48. Rolicka, A. et al. The chromatin-remodeling complexes B-WICH and NuRD regulate ribosomal transcription in response to glucose. *FASEB J.* **34**, 10818–10834 (2020).
49. Aydin, O. Z. et al. Human ISWI complexes are targeted by SMARCA5 ATPase and SLIDE domains to help resolve lesion-stalled transcription. *Nucleic Acids Res.* **42**, 8473–8485 (2014).
50. Xiao, A. et al. WSTF regulates the H2A.X DNA damage response via a novel tyrosine kinase activity. *Nature* **457**, 57–62 (2009).
51. Liu, Y. et al. WSTF acetylation by MOF promotes WSTF activities and oncogenic functions. *Oncogene* **39**, 5056–5067 (2020).
52. McGaughey, G. B., Gagne, M. & Rappe, A. K. pi-Stacking interactions. Alive and well in proteins. *J. Biol. Chem.* **273**, 15458–15463 (1998).
53. Sharif, S. B., Zamani, N. & Chadwick, B. P. BAZ1B the Protean Protein. *Genes (Basel)* **12**, 1541 (2021).
54. Gong, F. et al. Screen identifies bromodomain protein ZMYND8 in chromatin recognition of transcription-associated DNA damage that promotes homologous recombination. *Genes Dev.* **29**, 197–211 (2015).
55. Park, S. H. et al. Timely termination of repair DNA synthesis by ATAD5 is important in oxidative DNA damage-induced single-strand break repair. *Nucleic Acids Res.* **49**, 11746–11764 (2021).
56. Mortusewicz, O. & Leonhardt, H. XRCC1 and PCNA are loading platforms with distinct kinetic properties and different capacities to respond to multiple DNA lesions. *BMC Mol. Biol.* **8**, 81 (2007).
57. Shiomi, Y. & Nishitani, H. Control of Genome Integrity by RFC Complexes; Conductors of PCNA Loading onto and Unloading from Chromatin during DNA Replication. *Genes (Basel)* **8**, 52 (2017).
58. Park, S. H. et al. Short-range end resection requires ATAD5-mediated PCNA unloading for faithful homologous recombination. *Nucleic Acids Res.* **51**, 10519–10535 (2023).
59. Somyajit, K. et al. Redox-sensitive alteration of replisome architecture safeguards genome integrity. *Science* **358**, 797–802 (2017).
60. Andrs, M. et al. Excessive reactive oxygen species induce transcription-dependent replication stress. *Nat. Commun.* **14**, 1791 (2023).

61. Zellweger, R. et al. Rad51-mediated replication fork reversal is a global response to genotoxic treatments in human cells. *J. Cell Biol.* **208**, 563–579 (2015).
62. Oppikofer, M. et al. Non-canonical reader modules of BAZ1A promote recovery from DNA damage. *Nat. Commun.* **8**, 862 (2017).
63. Nusawardhana, A., Pale, L. M., Nicolae, C. M. & Moldovan, G. L. USP1-dependent nucleolytic expansion of PRIMPOL-generated nascent DNA strand discontinuities during replication stress. *Nucleic Acids Res* **52**, 2340–2354 (2024).
64. Huang, T. T. et al. Regulation of monoubiquitinated PCNA by DUB autocleavage. *Nat. Cell Biol.* **8**, 339–347 (2006).
65. Uhlmann, F., Cai, J., Gibbs, E., O'Donnell, M. & Hurwitz, J. Deletion analysis of the large subunit p140 in human replication factor C reveals regions required for complex formation and replication activities. *J. Biol. Chem.* **272**, 10058–10064 (1997).
66. Jumper, J. et al. Highly accurate protein structure prediction with AlphaFold. *Nature* **596**, 583–589 (2021).
67. Evans, R. et al. Protein complex prediction with AlphaFold-Multimer. Preprint at *bioRxiv* https://doi.org/10.1101/2021.10.04.463034 2021.10.04.463034 (2022).

Acknowledgements

We thank members of the Center for Genomic Integrity, Institute for Basic Science (IBS), for helpful discussions and comments on the manuscript. The Global PhD fellowship supported Eunjin Ryu (NRF-2017H1A2A1044961) and Yeongjae Kim (NRF-2018H1A2A1063189). This research was mainly supported by the Institute for Basic Science (IBS-R022-D1 for Kyungjae Myung). This work was also partially supported by the UNIST research fund (1.180063) and the Institute for Basic Science (IBS-R022-A1 for Orlando D. Schärer).

Author contributions

Y.K. and N.Y.H. performed most of the cell-based experiments. Y.K., N.Y.H., M.-S.K. and B.-G.K. performed Mass-spectrometry. Y.K. and G.Y. produced and analyzed AlphaFold2 models. Y.K. and N.K. performed live-cell imaging. Y.K., N.Y.H. and M.-S.K. generated cell lines. Y.K., E.R. and J.Y. performed protein purification and biochemical experiments. Y.K., N.Y.H., and S.K. designed the experiments and analyzed the data. Y.K. and S.K. composed the manuscript with input from all authors. S.K. and K.M. directed the project.

Competing interests

The authors declare no competing interests.

Additional information

Supplementary information The online version contains supplementary material available at https://doi.org/10.1038/s41467-024-55005-3.

Correspondence and requests for materials should be addressed to Sukhyun Kang.

Peer review information *Nature Communications* thanks Patrick Varga-Weisz and the other anonymous reviewer(s) for their contribution to the peer review of this work. A peer review file is available.